

# **Optical Frequency Comb for Ultracold Groundstate Molecules**

master thesis in physics

by

**Andreas Klinger**

submitted to the Faculty of Mathematics, Computer  
Science and Physics of the University of Innsbruck

in partial fulfillment of the requirements  
for the degree of Master of Science

Supervisor:  
a. Univ.-Prof. Dr. Hanns-Christoph Nägerl

Innsbruck, March 2011



## Abstract

This thesis reports on the construction of an Erbium-fiber frequency comb. The laser system consist of a mode-locked Erbium-fiber laser and an Erbium-fiber amplifier. The laser system emits ultrashort light pulses with a duration of 45 fs, a repetition rate of 100 MHz and an average power of 250 mW. By coupling those pulses into a highly nonlinear fiber, we try to broaden the spectrum to reach a width of more than an octave. Additionally, we report on a setup with which we are able to characterize ultrashort laser pulses.

Furthermore, we present results of the numerical simulation of the nonlinear Schrödinger equation, which describes the spectral broadening inside the highly nonlinear fiber.



## **Zusammenfassung**

Im Rahmen dieser Arbeit wird der Aufbau eines Erbium-Faser Frequenzkamms beschrieben. Das Lasersystem, bestehend aus einem modengekoppelten Erbium-Faser Laser und einem Erbium-Faser Verstärker, erzeugt Lichtpulse mit einer Dauer von 45 fs, einer Wiederholfrequenz von 100 MHz und einer Ausgangsleistung von 250 mW. Diese ultrakurzen Lichtpulse werden anschließend in eine hochgradig nicht-lineare Glasfaser eingekoppelt, in welcher versucht wird das Spektrum auf eine Breite von über einer Oktave zu erweitern. Zusätzlich wird der Aufbau eines FROG-Analysators, welcher zur Charakterisierung ultrakurzer Lichtpulse dient, beschrieben.

Weiters wurden im Rahmen dieser Arbeit numerische Simulationen der nichtlinearen Schrödingergleichung durchgeführt. Ergebnisse dieser Simulationen, welche die spektrale Verbreiterung in der hochgradig nichtlinearen Glasfaser beschreiben, werden präsentiert.



# Contents

<b>1 Introduction</b>	<b>9</b>
<b>2 Theoretical Background</b>	<b>15</b>
2.1 What is an Ultrashort Laser Pulse? . . . . .	15
2.2 Physical Phenomena in Optical Fibers . . . . .	17
2.2.1 Optical Losses . . . . .	17
2.2.2 Chromatic Dispersion . . . . .	17
2.2.3 Nonlinear Effects . . . . .	20
2.3 Pulse-Propagation in Optical Fibers . . . . .	22
2.3.1 The Propagation Equation . . . . .	22
2.3.2 Numerical Methods . . . . .	25
2.4 Measurement of Ultrashort Laser Pulses . . . . .	26
2.4.1 Autocorrelation . . . . .	26
2.4.2 FROG: Frequency-Resolved Optical Gating . . . . .	27
<b>3 Experimental Setup</b>	<b>31</b>
3.1 The Erbium-Fiber Laser . . . . .	31
3.1.1 Mode-Locking . . . . .	31
3.1.2 Repetition Rate and Total Dispersion . . . . .	32
3.1.3 Technical Details . . . . .	34
3.1.4 Practical Mode-Locking Concerns . . . . .	34
3.2 The Erbium-Fiber Amplifier . . . . .	35
3.2.1 Soliton-Effect Compression in Anomalous Dispersion Fiber . . . . .	37
3.2.2 Prism Compressor . . . . .	38
3.2.3 Technical Details . . . . .	40
3.3 Supercontinuum Generation . . . . .	40
3.3.1 Coupling the Pulses into the Highly Nonlinear Fiber . . . . .	40
3.3.2 Experimental Results . . . . .	41
3.4 FROG Setup . . . . .	43
<b>4 Conclusion and Outlook</b>	<b>45</b>
<b>A Matlab Source Code: Simulation of the Nonlinear Schrödinger Equation</b>	<b>47</b>
<b>B Calculation for SF-10 Prism Compressor</b>	<b>51</b>
<b>References</b>	<b>53</b>





## CHAPTER 1

### Introduction

In the past, spectroscopy experiments have relied on the measurement of wavelength rather than frequency. The measurement of wavelength with interferometers is fundamentally limited by unavoidable wavefront distortions to a few parts in  $10^{10}$  [Ude02]. To reach higher accuracy a direct measurement of the frequency is desired. The first approach to measure an absolute optical frequency were the so-called harmonic frequency chains. Those use a well defined microwave frequency (Cs-clock transition), which is transferred into the optical frequency range by generating higher harmonics. This known frequency can then be compared with the unknown optical frequency. The drawbacks of this method are clearly the huge technical challenge, the cost and the fact that one specific frequency chain has to be designed for every frequency that one desires to measure. In an impressive effort Schnatz et al. used this method to measure the  $^{40}\text{Ca } ^3P_1 - ^1S_0$  transition and reached a relative standard uncertainty of less than  $10^{-12}$  [Sch96].

A groundbreaking development was the use of a mode-locked laser for the measurement of optical frequencies [Rei99]. A mode-locked laser emits a pulse train with a fixed repetition rate  $f_{\text{rep}}$  as shown in Fig. 1.1. If one looks at the pulse train in the frequency domain, which is connected to the time domain by the Fourier transform, this corresponds to a comb of equally spaced delta functions. The absolute frequency of all comb lines is well defined by two radio frequencies, the repetition rate  $f_{\text{rep}}$  and the carrier-envelope offset (CEO) frequency  $f_{\text{CEO}}$ , which gives the offset of the first comb line to zero. The repetition rate can easily be measured by monitoring the pulse train, for example with a fast photodetector. The measurement and the control of the CEO frequency is less straight forward. In 1997 Theodor W. Hänsch wrote a proposal for a universal optical frequency comb synthesizer, in which he describes the technique of the f-2f interferometer to measure the  $f_{\text{CEO}}$  [Hän06]. He partly received the nobel price in 2005 for this invention. The requirement for the f-2f interferometer is a comb spectrum that spans at least an optical octave, thus a factor of two in frequency. The principle is shown in Fig. 1.2. By frequency doubling light from the lower frequency end of the spectrum in a nonlinear crystal and measuring the heterodyne radio frequency beat with the higher frequency end of the spectrum one gets exactly the offset frequency  $f_{\text{CEO}}$ . The first experimental realization was done by Diddams et al. [Did00].

## 1 Introduction

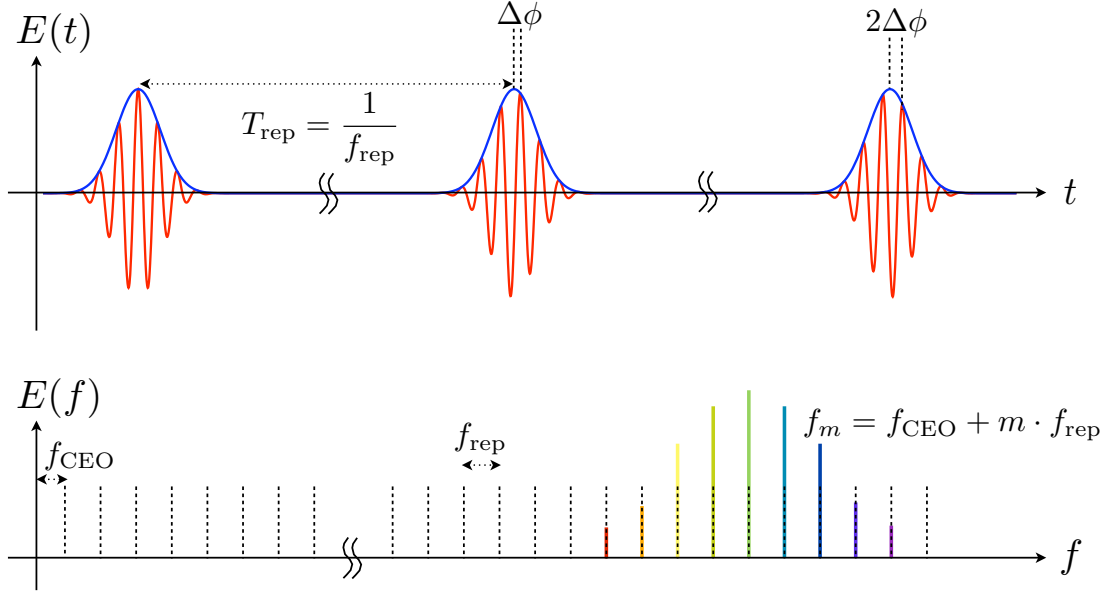


**Figure 1.1:** Top: The pulse train emitted by the mode-locked laser in the time domain. The pulses are separated by  $T_{\text{rep}}$ . The relative phase between the envelope and the electric field is given by  $\Delta\phi = 2\pi \frac{f_{\text{CEO}}}{f_{\text{rep}}}$ . Bottom: The Fourier transform of the field in time domain leads to the frequency comb. The comb is well defined by the two radio frequencies  $f_{\text{rep}}$  and  $f_{\text{CEO}}$ .

To measure an optical frequency with the frequency comb one just superimposes the comb light with the unknown laser light on a photo detector and measures the beat signal. One will observe the difference frequency between the laser frequency and the closest comb-line.

The first frequency combs have been realized by using mode-locked Ti:sapphire lasers [Ude99]. The output spectrum of such a laser typically spans up to 45 THz and is centered around 380 THz. To achieve an octave-spanning continuum, a so-called supercontinuum, the nonlinear spectral broadening in a microstructured silica fiber is usually used [Ran00].

In the early nineties also mode-locked fiber lasers were developed [Tam93]. In contrast to the bulky nature of mode-locked Ti:sapphire laser, fiber lasers have the advantages of less critical alignment, lower cost and more stable long term operation. But in terms of optical phase noise and output power, the Ti:sapphire laser used to be the better choice. More recently it has been shown that mode-locked fiber lasers can also compete in those areas. Schibli et al. have reached an average output power of more than 10 W and a relative linewidth in the submillihertz region with an Ytterbium-fiber comb [Sch08].

Since the development of the optical frequency comb technique there have been numerous applications. The applications range from precision spectroscopy [Hol00, Nie00, Rei00] to the development of optical atomic clocks [Did01, Ros08]. This new generation of clocks has reached relative uncertainties of  $10^{-17}$ . The preci-

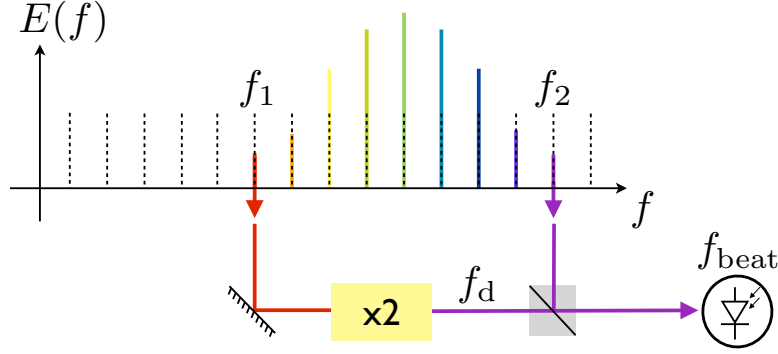


**Figure 1.2:** Schematic of the f-2f interferometer. Light from the lower end of the spectrum with frequency  $f_1 = f_{\text{CEO}} + m_1 \cdot f_{\text{rep}}$  is frequency doubled in a nonlinear crystal. The frequency doubled light with the frequency  $f_d = 2 \cdot f_{\text{CEO}} + 2 \cdot (m_1 \cdot f_{\text{rep}})$  is superimposed on a photodiode with light from the higher end of the spectrum with the frequency  $f_2 = f_{\text{CEO}} + m_2 \cdot f_{\text{rep}}$ . For  $m_2 = 2 \cdot m_1$ , the observed beat note  $f_{\text{beat}} = f_d - f_2$  is exactly the carrier-envelope offset frequency  $f_{\text{CEO}}$ .

sion has enabled measurements of the drift of fundamental constants [Biz03] and a test of general relativity [Cho10].

Our group at the University of Innsbruck is engaged in the study of ultracold atomic and molecular quantum gases. On the one hand, we are interested in using the frequency comb technique to precisely measure optical frequencies. On the other hand, we are using the technique to generate phase coherent radiation for a coherent state transfer of ultracold molecules.

Ultracold molecules offer numerous opportunities for interesting experiments in the context of precision measurements, quantum simulation, quantum information processing and cold controlled chemistry [Car09]. In particular, molecules that have a permanent electric dipole moment promise the realization of dipolar quantum gas systems [Gór02]. Many of these experiments, in particular the latter uses, require control over all the degrees of freedom of the molecules on the level of single quantum states. Control over the external degree of freedom implies that the sample should be close or even at quantum degeneracy. Thus far it has not been possible to directly cool molecules down to quantum degeneracy. One can achieve that by starting with a quantum degenerate sample of atoms. Via a Feshbach resonance these atoms can be associated to so-called "Feshbach molecules". A Feshbach molecule is an extremely weakly bound molecule, corresponding to the highest vibrational level right below the continuum. For reasons of collisional stability and to achieve a permanent electric dipole moment for heteronuclear molecules, it is necessary to transfer the molecules into the absolute ground state. It is mandatory to maintain control over the internal degrees of freedom i.e. the electronic, vibrational, rotational states of the molecules.

In the experiment, the molecules are coherently transferred from the highly excited vibrational state  $|a\rangle$  into the rovibrational ground-state  $|g\rangle$  via the Stimulated Raman

## 1 Introduction

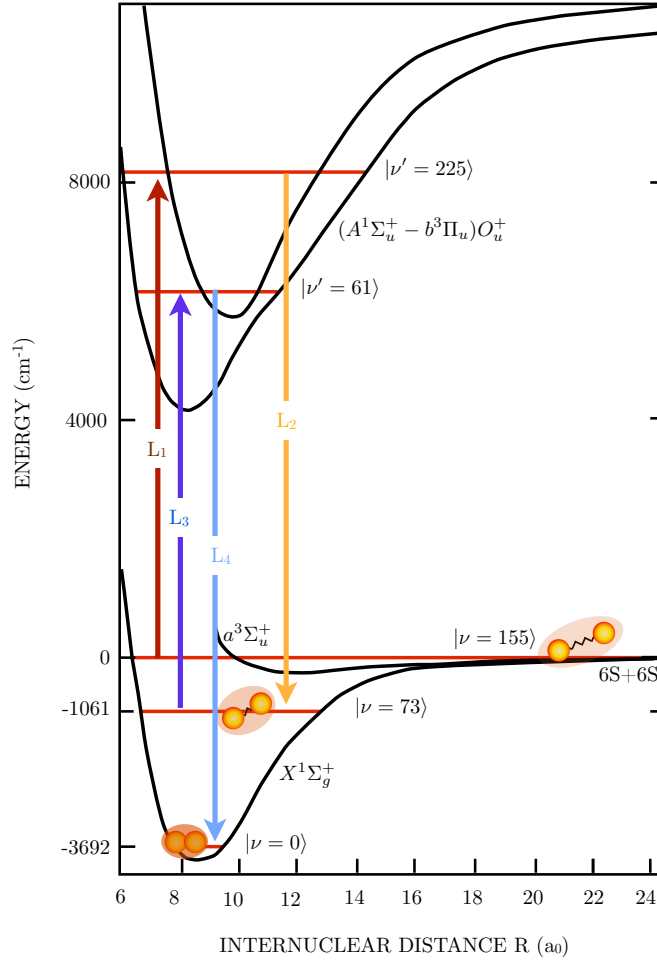


**Figure 1.3:** Molecular potentials and vibrational levels for transfer of  $\text{Cs}_2$  Feshbach molecules into the absolute ground-state. Initially the weakly bound Feshbach molecules are in state  $|\nu = 155\rangle$ . The transfer is achieved by a double STIRAP. The lasers  $L_1$  and  $L_2$  couple the Feshbach level  $|\nu = 155\rangle$  with the deeper bound level  $|\nu = 73\rangle$ .  $L_3$  and  $L_4$  couple  $|\nu = 73\rangle$  to the vibrational and rotational ground state  $|\nu = 0\rangle$  of the singlet  $X^1\Sigma_g^+$  potential. Figure taken from [Dan10].

Adiabatic Passage (STIRAP) technique (Fig. 1.3). The transfer is achieved by coupling to a third excited level, as indicated in Fig. 1.4. The STIRAP technique relies on the existence of a dark state  $|d\rangle = \cos \Theta \cdot |g\rangle - \sin \Theta \cdot |a\rangle$  whereas  $\Theta$  is given by  $\tan \Theta = \Omega_1(t)/\Omega_2(t)$ .  $\Omega_1$  and  $\Omega_2$  are the time dependent Rabi frequencies of laser 1, which couples the initial molecular state  $|a\rangle$  to an excited state  $|e\rangle$ , and laser 2, which couples  $|g\rangle$  to  $|e\rangle$ .

By applying a counterintuitive pulse sequence, shown in Fig. 1.4, the population is adiabatically transferred from state  $|a\rangle$  to state  $|g\rangle$  without ever populating the excited state  $|e\rangle$ . In theory, an efficiency of 100% is possible. The "intuitive" counterpart, for

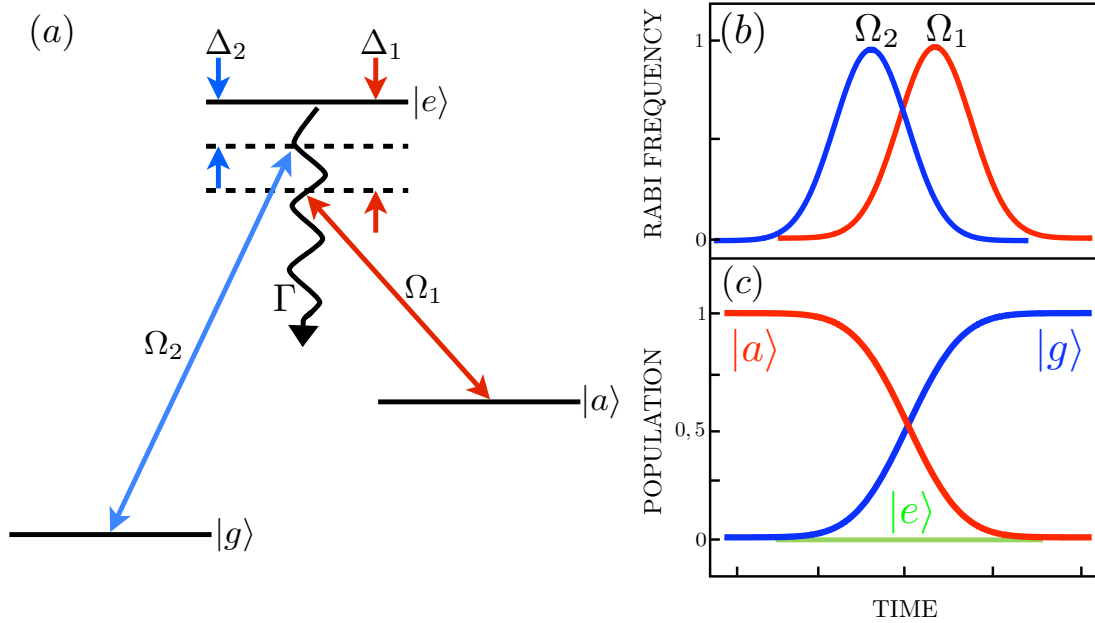


**Figure 1.4:** (a) A simplified levels scheme for the STIRAP process. Initially the molecules are in state  $|a\rangle$  and are then transferred to state  $|g\rangle$ . (b) The Rabi frequencies of the two lasers. Counterintuitively, laser 2 is turned on earlier. (c) The state population during the process. Note that the excited state  $|e\rangle$  is never populated.

which the population is pumped into state  $|e\rangle$  and from there pumped down to state  $|g\rangle$ , would reach only 33%.

A crucial point during STIRAP transfer is the requirement for adiabaticity. The criterion for the adiabaticity is  $\tau_p \cdot \Omega^2 \gg (2\pi)^2 \cdot \Gamma$ , where  $\Omega \approx \Omega_1 \approx \Omega_2$ ,  $\tau_p$  the transfer time and  $\Gamma$  the decay rate from the excited state  $|e\rangle$  [Ber98]. The Rabi frequencies have to be sufficiently high, and the time during which the Rabi frequencies overlap has to be long enough. This criterion puts stringent requirements on the STIRAP laser performance, especially on the relative phase noise between the two lasers. The energy difference between state  $|a\rangle$  and state  $|g\rangle$  which corresponds to the frequency difference between laser 1 and laser 2, is on the order of 100 THz. To achieve low phase noise between the STIRAP lasers, it is on the one hand possible to lock them independently to a cavity. Otherwise it is possible to stabilize the relative phase noise by referencing both of them to the same frequency comb.

By locking the STIRAP lasers to a Ti:sapphire frequency comb, the group of D. S. Jin and J. Ye has produced ultracold dense samples of KRb ground-state molecules [Ni08]. In Innsbruck, Danzl et al. have locked the STIRAP lasers to a cavity for short term stability and also referenced them to an Erbium-fiber frequency comb for long term stability and reproducibility and so produced ultracold dense samples of  $\text{Cs}_2$  ground-state molecules [Dan08, Dan10]. Lang et al. have created  $\text{Rb}_2$  triplet molecules close to degeneracy without a frequency comb by Pound-Drever-Hall locking the

## 1 Introduction

STIRAP lasers to a single cavity [Lan08]. More recently Aikawa et al. have transferred initially photoassociated KRb molecules into the absolute ground-state also by locking the STIRAP lasers to a cavity [Aik10].

The goal of this thesis is to build an Erbium-fiber frequency comb and to establish the technical know-how at the University of Innsbruck. This kind of laser system is also commercially available e.g. from Menlo Systems\* and Toptica†. The laser system consists of an Erbium-fiber laser, an Erbium-fiber amplifier and a highly nonlinear fiber for supercontinuum generation [Tau03, Tau04b]. The advantage of being able to produce homebuilt lasers is clearly the lower cost and the opportunity to adjust the performance and all significant parameters, e.g. the comb spectrum, to be suitable for a specific experiment.

This thesis is structured as follows. It starts with a theoretical section that reviews the physics of ultrashort laser pulses and the propagation of pulses in optical fibers. It includes a numerical simulation of the propagation equation, which is used for the simulation of the spectral broadening in a highly nonlinear fiber. Afterwards follows a chapter that describes the experimental work that has been done. It describes the setup and the performance of the Erbium-fiber ring oscillator and the subsequent amplifier. Afterwards the results of the spectral broadening in a piece of highly nonlinear fiber are presented. An additional part describes the setup of FROG, a device to characterize ultrashort laser pulses.

---

\*<http://www.menlosystems.com>

†<http://www.toptica.com>

## CHAPTER 2

### Theoretical Background

This chapter reviews the essential physics of mode-locked fiber lasers. It starts with a mathematical description of ultrashort lasers pulses. The following section describes the physical phenomena in optical fibers. It covers the optical losses, the chromatic dispersion and the nonlinearities. Afterwards follows a derivation of the propagation equation and a description of one method to solve this equation numerically. The propagation equation, also known as nonlinear Schrödinger equation, describes the propagation of short light pulses inside an optical fiber. The chapter concludes with the theory of ultrashort pulse measurement. The deliberations in this chapter are based on two great books, one on nonlinear fiber optics by G. P. Agrawal and the other one on ultrashort pulse measurement by R. Trebino [Agr89, Tre02].

### 2.1 What is an Ultrashort Laser Pulse?

Simply put, it is a really short burst of electro-magnetic energy. Mathematically one can describe such a pulse like any other electro-magnetic wave by the electric field  $E(x, y, z, t)$ . For a cw-laser the electric field would just be sinusoidal in time. For an ultrashort pulse it is a product of a sine wave and a pulse-envelope function. An example is shown in Fig. 2.1.\*

$$\mathcal{E}(t) = \frac{1}{2} \left( \sqrt{I(t)} \cdot \exp(i(\omega_0 t - \phi(t))) + c.c. \right), \quad (2.1)$$

where  $I(t)$  and  $\phi(t)$  are the time dependent intensity and the phase of the pulse and  $t$  is the time.  $\omega_0$  is the carrier angular frequency, it is on the order of  $10^{15} \text{ s}^{-1}$ . For convenience one can define a complex amplitude of the pulse

$$E(t) = \sqrt{I(t)} \cdot \exp(-i\phi(t)), \quad (2.2)$$

where the intensity of the pulse is given by

$$I(t) = |E(t)|^2 \quad (2.3)$$

and the temporal phase is given by

$$\phi(t) = -\arctan \left( \frac{\text{Im}(E(t))}{\text{Re}(E(t))} \right). \quad (2.4)$$

---

\*and let us ignore the vector character of the electric field and the spatial portion of the field

## 2 Theoretical Background

One can also describe the pulse in frequency domain, which is related to the time domain via Fourier transform:

$$\tilde{\mathcal{E}}(\omega) = \int_{-\infty}^{\infty} \mathcal{E}(t) \exp(-i\omega t) dt. \quad (2.5)$$

To go back to the time domain one has to perform an inverse Fourier transform

$$\mathcal{E}(t) = \frac{1}{2\pi} \int_{-\infty}^{\infty} \tilde{\mathcal{E}}(\omega) \exp(i\omega t) d\omega. \quad (2.6)$$

Analogous to the function in time domain one can write the function  $\tilde{\mathcal{E}}(\omega)$  as

$$\tilde{\mathcal{E}}(\omega) = \sqrt{S(\omega)} \cdot \exp(-i\varphi(\omega)), \quad (2.7)$$

where  $S(\omega)$  is the intensity in frequency domain, commonly known as the spectrum, and  $\varphi(\omega)$  is the spectral phase. So what are the temporal and the spectral phase and how can we think about them? One can simply expand the phase in a Taylor series and look at the terms in detail. Pulses with different phase distortions are shown in Fig. 2.2.

$$\phi(t) = \phi_0 + \phi_1 \cdot t + \frac{1}{2} \cdot \phi_2 \cdot t^2 + \frac{1}{6} \cdot \phi_3 \cdot t^3 + \dots \quad (2.8)$$

Let us consider a pulse with only zeroth-order phase, meaning that the temporal phase is a constant function of  $t$ . Due to Fourier transform this automatically implies that the spectral phase is a constant function of  $\omega$ . A pulse like this is called a Fourier-limited pulse. That is because for a certain spectrum there is a minimum pulse duration and the pulse cannot be any shorter than that. There is a quantity called the time-bandwidth product (TBP).

$$\text{TBP} = \Delta t \cdot \Delta f \quad (2.9)$$

where  $\Delta t$  and  $\Delta f$  are the FWHM in time and frequency domain. In general one can say that a higher TBP indicates a more complex pulse. For a Fourier-limited Gaussian pulse the TBP is 0.44.

If we consider a first-order phase in time, the consequence is a shift of the spectrum. And of course a linear term in the spectral phase shifts the pulse in time, which is something one does not really care about. For a train of pulses it does not really matter if these pulses arrive a little sooner or later.

A second-order phase is commonly known as linear chirp. As an example let us consider a pulse with constant phase. As this pulse travels through a medium it will develop a quadratic phase in time and frequency space due to the different phase velocities. The spectrum does not change, but the temporal pulse envelope broadens. The electric field oscillates with the carrier frequency at the center of the pulse. The leading (trailing) edge will oscillate at higher (lower) frequencies, depending on the sign of the chirp. The TBP is now larger than 0.44.

In materials with higher order dispersion also third order spectral phase distortions can happen. In this case the carrier frequency is on one side of the pulse and the higher



and lower frequencies are at the other end. Those frequencies beat with each other and produce intensity fluctuations. And of course there are even higher order phase distortions. The phase of a real laser pulse is usually a combination of all orders of phases.

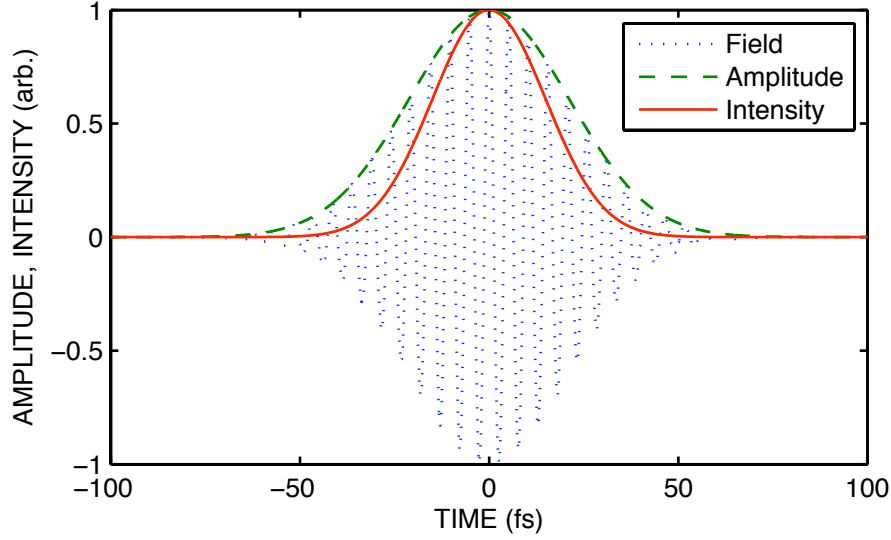


**Figure 2.1:** This plot shows the fast oscillating electric field, the amplitude and the intensity of a gaussian pulse with a constant temporal phase.

## 2.2 Physical Phenomena in Optical Fibers

### 2.2.1 Optical Losses

The optical loss is modeled by an exponential decay

$$P_T = P_0 \cdot \exp(-\alpha L), \quad (2.10)$$

where  $P_T$  is the transmitted power,  $P_0$  the power that is launched into the fiber,  $\alpha$  the attenuation constant and  $L$  the fiber length.  $\alpha$  depends on the wavelength and has a minimum of about 0.2 dB/km at  $1.55 \mu\text{m}$  but can be as high as 10 dB/km at visible wavelengths. The loss is dominated by material absorption and Rayleigh scattering. However, optical losses are an important issue in telecommunications. For fiber lasers, as discussed here, optical loss is usually not really relevant and can be neglected.

### 2.2.2 Chromatic Dispersion

Every kind of oscillator has a different response to different driving frequencies. This is also true for the bound electrons of a dielectric medium, which interact with electromagnetic radiation. For that reason the refractive index  $n(\omega)$  is frequency dependent.

## 2 Theoretical Background

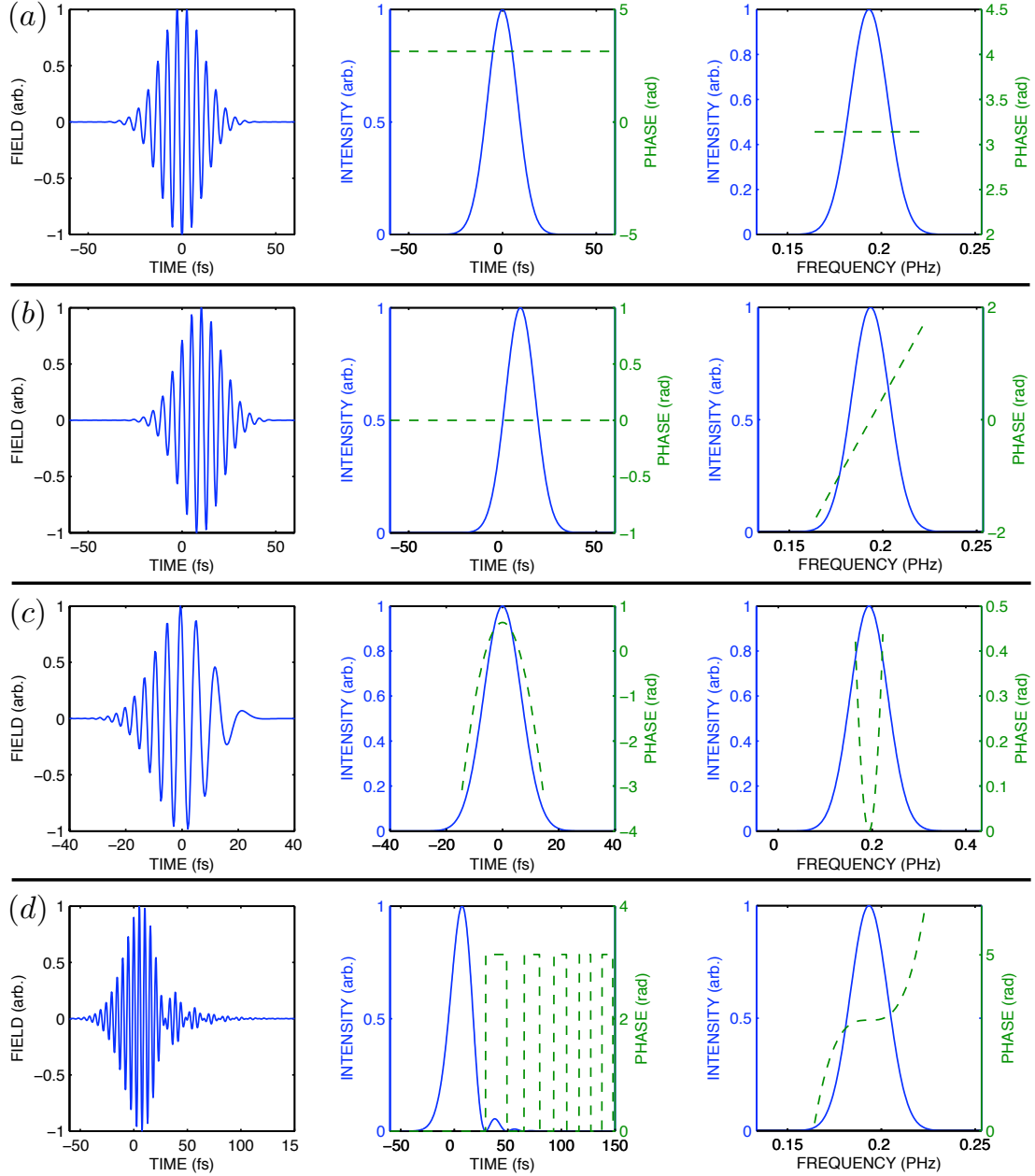


**Figure 2.2:** Gaussian pulses with different phase distortions. (a) Fourier limited pulse. The phase (dashed) is constant in time and frequency domain. The frequency of the electric field does not change over the length of the pulse. (b) Linear phase in frequency domain. The pulse is shifted in time domain. (c) Positive linear chirp, the phase is quadratic. The frequency of the electric field changes over the length of the pulse. (d) Cubic phase in frequency domain. The carrier frequency is located at the left side of the pulse, the higher and lower frequency components are located on the right side. The beat between them causes the intensity fluctuations.

The speed of light in a medium (phase velocity) is given by  $c/n(\omega)$ , so different wavelengths travel with different speeds. For pulses that are a superposition of multiple frequencies chromatic dispersion has the effect of pulse broadening.

The refractive index dependence on  $\omega$  can be modeled by the empiric Sellmeier equation

$$n^2(\omega) = 1 + \sum_{i=1}^m \frac{B_i \omega_i^2}{\omega_i^2 - \omega^2}. \quad (2.11)$$

The Sellmeier equation can also be written in the more common wavelength dependent form

$$n^2(\lambda) = 1 + \frac{B_1 \lambda^2}{\lambda^2 - C_1} + \frac{B_2 \lambda^2}{\lambda^2 - C_2} + \frac{B_3 \lambda^2}{\lambda^2 - C_3}, \quad (2.12)$$

where  $B_i$  and  $C_i$  are the experimentally determined Sellmeier coefficients.

For a mathematical description it is useful to define a mode-propagation constant  $\beta$  (also used in Eq. 2.36 below) and perform a Taylor series around the frequency  $\omega_0$ .

$$\beta(\omega) = n(\omega) \frac{\omega}{c} = \beta_0 + \beta_1(\omega - \omega_0) + \frac{1}{2}\beta_2(\omega - \omega_0)^2 + \dots, \quad (2.13)$$

where

$$\beta_n = \left( \frac{d^n \beta}{d\omega^n} \right)_{\omega=\omega_0}. \quad (2.14)$$

The reason why one wants to do this Taylor expansion is that those coefficients  $\beta_n$  have illustrative physical interpretations.

$\beta_1$  is related to the group velocity of the pulse by the relation  $v_g = \frac{1}{\beta_1}$ . The group velocity is the velocity with which the envelope of the pulse travels.

$\beta_2$  causes a quadratic phase distortion in frequency domain, it chirps the pulse (Fig. 2.2(c)). For an initially unchirped pulse this has the effect of temporal broadening.  $\beta_2$  is often called the group-velocity dispersion (GVD) parameter.

$\beta_3$  causes a cubic phase distortion of a pulse. The pulse develops intensity fluctuations at the leading or the trailing edge, dependent on the sign of  $\beta_3$  (Fig. 2.2(d)).

For fiber laser applications  $\beta_1$  and  $\beta_2$  usually dominate and in the case of  $\beta_2 \simeq 0$ ,  $\beta_3$  has to be taken into account. Higher orders can be neglected in this work.

Instead of  $\beta_2$  one can also define the dispersion parameter  $D$ , which is often used in fiber-optics literature.

$$D = \frac{d\beta_1}{d\lambda} = -\frac{2\pi c}{\lambda^2} \beta_2 \quad (2.15)$$

One can distinguish between two regimes. A fiber is said to have normal dispersion when  $\beta_2 > 0$ , which means that the red components of a pulse travel faster than the blue components. The other regime where  $\beta_2 < 0$  is called anomalous-dispersion regime. A formula that is useful and easy to remember is the dispersion length

$$L_D = \frac{T_0^2}{|\beta_2|}. \quad (2.16)$$

## 2 Theoretical Background

$T_0$  is the half-width at the 1/e-intensity point, for a gaussian pulse  $T_{\text{FWHM}} \approx 1.665 \cdot T_0$ .  $L_D$  is the length where dispersion starts to matter, more precisely this is the distance after which a gaussian pulse has temporarily broadened by a factor of  $\sqrt{2}$ .

### 2.2.3 Nonlinear Effects

Nonlinear effects appear if the induced polarization  $\vec{P}$  responds nonlinearly to the electric field  $\vec{E}$

$$\vec{P} = \epsilon_0 \left( \chi^{(1)} \cdot \vec{E} + \chi^{(2)} : \vec{E}\vec{E} + \chi^{(3)} : \vec{E}\vec{E}\vec{E} + \dots \right) \quad (2.17)$$

where  $\epsilon_0$  is the vacuum permittivity and  $\chi^{(i)}$  is the  $i$ th order susceptibility. Second order susceptibility is responsible for nonlinear effects such as second-harmonic generation (SHG) and sum-frequency generation. Typically second-order effects do not occur in fibers because  $\chi^{(2)}$  vanishes for silica glasses.

So the lowest-order nonlinear effects that happen in fibers are caused by the third-order susceptibility  $\chi^{(3)}$ . Basically one distinguishes between third-harmonic-generation (THG), optical Kerr-effect (nonlinear refraction) and four-wave-mixing. THG and four-wave-mixing are usually not efficient in optical fibers because phase matching between driving field and generated field is not preexisting.

The most important nonlinear effect for this work is nonlinear refraction. This effect describes the intensity dependence of the refractive index, which can be expressed by

$$\bar{n}(\omega, |E|^2) = n(\omega) + n_2 |E|^2 \quad (2.18)$$

where  $n$  is the linear index of refraction and  $n_2$  is the nonlinear-index coefficient, which is proportionally related to  $\chi^{(3)}$ . This intensity dependence causes interesting effects such as self-phase modulation (SPM) and cross-phase modulation (XPM).

SPM is an effect where the pulse itself induces a varying index of refraction. The center of the pulse causes a higher change in the index than the edges of the pulse. This varying index of refraction shifts the leading edge of the pulse to lower frequencies and the trailing edge to higher frequencies. Those generated frequencies cause a broadening in the spectrum of the pulse, but do not effect the temporal envelope of the pulse. Similar to the dispersion length a nonlinear length can be defined.

$$L_{\text{NL}} = \frac{1}{\gamma \cdot P_0}, \quad (2.19)$$

where  $P_0$  is the peak intensity and  $\gamma$  the nonlinearity coefficient which is given by

$$\gamma = \frac{n_2 \cdot \omega_0}{c \cdot A_{\text{eff}}}, \quad (2.20)$$

where  $A_{\text{eff}}$  is known as the effective core area. For gaussian fiber modes it can be written as

$$A_{\text{eff}} = \pi \cdot w^2, \quad (2.21)$$

where  $w$  is the half width of the gaussian mode and depends on the fiber parameters.

With  $L_D$  and  $L_{NL}$  one can easily determine which effects dominate within a certain fiber length and for a certain pulse. If  $L_D$  and  $L_{NL}$  are both small compared to the total fiber length the interplay between dispersion and non-linearity can lead to a different behavior than one of this effects on its own. For the case  $\beta_2 < 0$  optical solitons can occur.

### Optical Solitons

An optical soliton is a wave packet that is able to travel for a long distance without distortion. Solitons can be investigated by solving the propagation equation (Eq. 2.49 below) with the inverse scattering method [Agr89], or by doing a numerical simulation of the propagation equation e.g. with the split-step Fourier method.

Simply put, for a certain ratio of  $L_D$  and  $L_{NL}$  the phases from SPM and GVD cancel each other, and the wave packet travels undistorted. This happens for integer numbers of  $N$  whenever

$$N^2 = \frac{L_D}{L_{NL}}. \quad (2.22)$$

Let us consider a hyperbolic secant pulse:

$$P(t) = P_0 \cdot \text{sech}^2\left(\frac{t}{\tau}\right) \quad (2.23)$$

where  $P_0$  is the peak power and  $\tau$  is the width,  $t_{FWHM} = 1.76 \cdot \tau$ . The condition for the pulse to evolve as a fundamental ( $N=1$ ) soliton is

$$P_0 = P_{(N=1)} = \frac{|\beta_2|}{\gamma T_0^2} \quad (2.24)$$

to support a higher-order soliton ( $N = 2, 3, 4, \dots$ ), the peak power has to be higher (can easily be calculated with Eq. 2.22). Higher order solitons evolve in a periodic pattern, they go through an initial narrowing phase and recover to their old shape after one soliton period. Fig. 2.3 shows the evolution of a second order soliton.

## 2 Theoretical Background

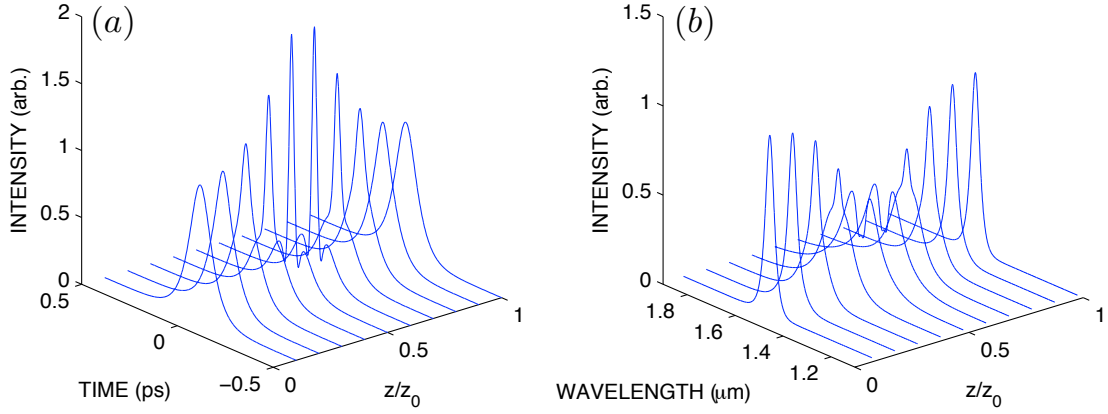


**Figure 2.3:** Result of the simulation of a second-order optical soliton plotted for one soliton period  $z_0$ . The simulation was done with the Matlab source code from App. A. Chosen fiber parameters:  $\beta_2 = -2 \cdot 10^{-26} \text{ s}^2/\text{m}$ ,  $\beta_3 = 0$ ,  $\gamma = 1 \cdot 10^{-3} \text{ /W/m}$ . Initial hyperbolic secant pulse parameters:  $P_0 = 31867 \text{ W}$ ,  $\tau = 50 \text{ fs}$ . After one soliton period the pulse is exactly the same as in the beginning. (a) Evolution of the pulse in time domain. (b) Evolution of the pulse spectrum.

## 2.3 Pulse-Propagation in Optical Fibers

### 2.3.1 The Propagation Equation

To understand and simulate the physical processes and phenomena of pulses in optical fibers it is useful to create a mathematical formalism. Basically, the whole problem is described by Maxwell's equations of a dielectric media without free charges and free currents:

$$\nabla \times \vec{E} = -\frac{\partial \vec{B}}{\partial t}, \quad (2.25)$$

$$\nabla \times \vec{H} = \frac{\partial \vec{D}}{\partial t}, \quad (2.26)$$

$$\nabla \cdot \vec{D} = 0, \quad (2.27)$$

$$\nabla \cdot \vec{B} = 0, \quad (2.28)$$

where  $\vec{E}$  and  $\vec{H}$  describe the electric and the magnetic field and  $\vec{D}$  and  $\vec{B}$  are the corresponding flux densities.

$$\vec{D} = \epsilon_0 \vec{E} + \vec{B}, \quad (2.29)$$

$$\vec{B} = \mu_0 \vec{H} + \vec{M}, \quad (2.30)$$

### 2.3 Pulse-Propagation in Optical Fibers

where  $\epsilon_0$  is the vacuum permittivity,  $\mu_0$  the vacuum permeability,  $\vec{P}$  the induced electric polarization and  $\vec{M}$  the induced magnetic polarization.

Maxwell's equations can be used to obtain the wave equation

$$\nabla \times \nabla \times \vec{E} = -\frac{1}{c^2} \frac{\partial^2 \vec{E}}{\partial t^2} - \mu_0 \frac{\partial^2 \vec{P}}{\partial t^2}. \quad (2.31)$$

As  $\vec{P}$  (phenomenologically described in Eq. 2.17) is not linear in  $\vec{E}$ , one way is to treat  $P_{\text{NL}}$  the nonlinear part of  $\vec{P}$  as a perturbation and first solve the equation for  $P_{\text{NL}} = 0$ . With this assumption and after transforming to frequency space Eq. 2.31 has the form:

$$\nabla \times \nabla \times \tilde{\vec{E}}(\vec{r}, \omega) = -\epsilon(\omega) \frac{\omega^2}{c^2} \tilde{\vec{E}}(\vec{r}, \omega). \quad (2.32)$$

$\epsilon(\omega)$  is in general a complex number where the real part is related to the index of refraction and the imaginary part is related to the absorption coefficient. As the absorption is small enough one can replace  $\epsilon(\omega)$  by  $n^2(\omega)$ . With the identity

$$\nabla \times \nabla \times \vec{E} = \nabla(\nabla \cdot \vec{E}) - \nabla^2 \vec{E} \quad (2.33)$$

and Eq. 2.27 one obtains

$$\nabla^2 \tilde{\vec{E}}(\vec{r}, \omega) = -n^2(\omega) \frac{\omega^2}{c^2} \tilde{\vec{E}}(\vec{r}, \omega). \quad (2.34)$$

Now, because of the symmetry of the fiber it is convenient to write the equation in cylindrical coordinates:

$$\frac{\partial^2 \tilde{\vec{E}}}{\partial \rho^2} + \frac{1}{\rho} \frac{\partial \tilde{\vec{E}}}{\partial \rho} + \frac{1}{\rho^2} \frac{\partial^2 \tilde{\vec{E}}}{\partial \phi^2} + \frac{\partial^2 \tilde{\vec{E}}}{\partial z^2} + n^2 k_0^2 \tilde{\vec{E}} = 0, \quad (2.35)$$

with  $k_0 = \omega/c$ . One can then separate the radial and the axial part using the ansatz:

$$\tilde{\vec{E}}(\vec{r}, \omega) = A(\omega) F(\rho) \exp(im\phi) \exp(i\beta z) \quad (2.36)$$

with the normalization constant  $A$ , the radial field  $F$ , an integer number  $m$  and the propagation constant  $\beta$ . So the radial equation is given by

$$\frac{d^2 F}{d\rho^2} + \frac{1}{\rho} \frac{dF}{d\rho} + (n^2 k_0^2 - \beta^2 - \frac{m^2}{\rho^2}) F = 0. \quad (2.37)$$

For a step index fiber with core radius  $a$  the refractive index is  $n_1$  for  $\rho \leq a$  and  $n_2$  for  $\rho > a$ . The solutions of this equation are in principle Bessel and Neumann functions. By solving this equation one can also see that the number of transversal modes that are supported by the fiber are given by the parameters  $a$ ,  $n_1$  and  $n_2$ . It shows that for a small core radius the fiber supports just one single mode. One can define the fiber parameter

$$V = k_0 \cdot a \sqrt{n_1^2 - n_2^2}. \quad (2.38)$$

## 2 Theoretical Background

For  $V < 2.405$  a fiber is a single mode fiber. In this project only single mode fibers are used. For convenience this mode can be approximated by a gaussian function. There is a relation<sup>†</sup> between the width of the gaussian and  $V$  which can be useful to estimate for example  $A_{\text{eff}}$  from Eq. 2.21.

To describe the propagation of pulses as they appear in an Erbium-fiber laser the nonlinearity can not be neglected. One has to include that in the propagation equation. By splitting the polarization  $\vec{P}$  into a linear and a nonlinear part, Eq. 2.31 can be written as

$$\nabla^2 \vec{E} - \frac{1}{c^2} \frac{\partial^2 \vec{E}}{\partial t^2} = -\mu_0 \frac{\partial^2 \vec{P}_L}{\partial t^2} - \mu_0 \frac{\partial^2 \vec{P}_{NL}}{\partial t^2}. \quad (2.39)$$

To solve this equation one has to make some simplifying assumptions.  $P_{NL}$  has to be small compared to  $P_L$ , the width of the spectrum  $\Delta\omega$  is small compared to  $\omega_0$  which implies that the temporal pulse width is not shorter than 0.1 ps. It is useful to write the electric field as a product of a slowly varying part  $\vec{E}$  and a fast oscillating part. This is called the Slowly Varying Envelope Approximation (SVEA), for which one assumes that the envelope is varying slowly compared to the oscillations of the electric field.

$$\vec{E}(\vec{r}, t) = \frac{1}{2} \vec{e}_x (\vec{E}(\vec{r}, t) \exp(-i\omega_0 t) + c.c.) \quad (2.40)$$

Now one needs a relation for  $P_{NL}$ . In general  $P_{NL}$  is described by this complicated integral, but if one assumes that the response of  $\chi^{(3)}(t)$  is instantaneous one can write

$$\vec{P}_{NL}(\vec{r}, t) = \epsilon_0 \chi^{(3)} : \vec{E}(\vec{r}, t) \vec{E}(\vec{r}, t) \vec{E}(\vec{r}, t). \quad (2.41)$$

Eq. 2.40 plugged into Eq. 2.41 shows that the nonlinear polarization oscillates at  $\omega_0$  and at  $3\omega_0$ . One can typically ignore the third-harmonic generation as this process is not phase-matched and not effective. Again one can do the SVEA and get the following expression for the slowly varying part.

$$\vec{P}_{NL} \simeq \epsilon_0 \epsilon_{NL} \vec{E}(\vec{r}, t) \quad (2.42)$$

with

$$\epsilon_{NL} = \frac{3}{4} \chi^{(3)} |\vec{E}(\vec{r}, t)|^2. \quad (2.43)$$

Now, one can substitute Eq. 2.42 and an expression for  $P_L$  into Eq. 2.39. Again one can go to frequency domain, but now there is the problem that  $\epsilon_{NL}$  is intensity dependent, which makes the equation nonlinear. One possibility is to assume that  $\epsilon_{NL}$  is a constant, it is small anyway. With this trick one finds the equation for the slowly varying envelope in frequency space.

$$\nabla^2 \tilde{E} + \epsilon(\omega) k_0^2 \tilde{E} = 0 \quad (2.44)$$

---

<sup>†</sup> this relation can be found on page 35 in [Agr89]



with

$$\epsilon(\omega) = 1 + \chi^{(1)}(\omega) + \epsilon_{\text{NL}} \quad (2.45)$$

and Eq. 2.44 can again be solved by separating the variables using the ansatz

$$\tilde{E}(\vec{r}, \omega - \omega_0) = F(x, y) \tilde{A}(z, \omega - \omega_0) \exp(i\beta_0 z). \quad (2.46)$$

This leads again to two equations for the radial and the axial function.

$$2i\beta_0 \frac{\partial \tilde{A}}{\partial z} + (\bar{\beta} - \beta_0^2) \tilde{A} = 0 \quad (2.47)$$

$\bar{\beta}$  can be evaluated from the radial equation. After performing an inverse Fourier transformation one ends up with the propagation equation.

$$\frac{\partial A}{\partial z} + \beta_1 \frac{\partial A}{\partial t} + \frac{i}{2} \beta_2 \frac{\partial^2 A}{\partial t^2} = i\gamma |A|^2 A \quad (2.48)$$

Further, it is convenient to go to the moving frame of the pulse as one cares about the evolution of the pulse. The  $\beta_1$ -term is responsible for the group velocity. With the transformation  $T = t - \beta_1 z$  one transforms to the moving frame of the pulse. So the equation is

$$\frac{\partial A}{\partial z} + \frac{i}{2} \beta_2 \frac{\partial^2 A}{\partial T^2} = i\gamma |A|^2 A. \quad (2.49)$$

This equation contains the  $\beta_2$ -term that describes the GVD, and the nonlinear term on the right side. The absorption term has been dropped. This equation is an example of the nonlinear Schrödinger equation (NLSE). With  $z$  and  $T$  interchanged, it is essentially the Gross-Pitaevskii equation of matter wave physics [Gro61].

In the next chapter this equation is used for some simulations, whereas for pulses that are shorter than 100 fs some of the assumptions made are questionable. In that case it is more precise to use the generalized propagation equation [Liu07, Mus05].

$$\frac{\partial A}{\partial z} + \frac{i}{2} \beta_2 \frac{\partial^2 A}{\partial T^2} - \frac{1}{6} \beta_3 \frac{\partial^3 A}{\partial T^3} = i\gamma \left( |A|^2 A + \frac{2i}{\omega_0} \frac{\partial}{\partial T} (|A|^2 A) - T_R A \frac{\partial |A|^2}{\partial T} \right) \quad (2.50)$$

This equation contains three additional terms. The  $\beta_3$ -term describes third order dispersion, the second term on the right side is responsible for self-steepening and the third term for a self-frequency shift ( $T_R \approx 5$  fs).

### 2.3.2 Numerical Methods

To perform a simulation of Eq. 2.49 one can use the split-step Fourier method (SSFM) [Agr89]. Eq. 2.49 can be rearranged in the following way

$$\frac{\partial A}{\partial z} = (\hat{D} + \hat{N})A, \quad (2.51)$$

## 2 Theoretical Background

where  $\hat{D} = -\frac{i}{2}\beta_2 \frac{\partial^2}{\partial T^2}$  stands for the dispersion operator and  $\hat{N} = i\gamma|A|^2$  for the nonlinear operator. In reality those two operators act together all the time, for numerical simulations one can assume that for a very short interval  $h$  nonlinearity and dispersion act independently. So one can write

$$A(z+h) \approx \exp(h\hat{N}) \exp(h\hat{D})A(z). \quad (2.52)$$

Further, it is convenient to let the dispersion operator act in frequency space, because the time derivative just becomes a multiplication with  $i\omega$ . An improved version of this method is the so called symmetrized split-step Fourier method where the nonlinearity acts in the middle of each step, and not at the end.

$$A(z+h) \approx \exp(h/2\hat{D}) \exp(h\hat{N}) \exp(h/2\hat{D})A(z) \quad (2.53)$$

For even more accuracy the operator  $\exp(h\hat{N})$  can be replaced by  $\exp(\int_z^{z+h} \hat{N}(z')dz')$  which has to be calculated by an iterative process, as  $\hat{N}(z+h)$  is not known.

The Matlab source code that runs a simulation of the NLSE with the symmetrized SSFM can be found in App. A. The simulation uses Eq. 2.49 but with the additional third-order dispersion term taken into account. The Fast Fourier Transform (FFT) algorithm is used to perform the Fourier transformations.

## 2.4 Measurement of Ultrashort Laser Pulses

The measurement of ultrashort pulses is an important topic when building a mode-locked laser. It is absolutely necessary to be able to precisely characterize the pulses coming out of the laser. The problem in measuring really short pulses is the lack of a really fast detector. To measure a time event one has to resolve it somehow with a faster time event. To take a picture of some object the resolution of the optics has to be higher than the smallest features of the object to resolve them properly. The pulses that occur in this project are as short as 45 fs. This is the shortest event in our lab. So let us use the shortest event that exists in the lab to measure the pulse, which is the pulse itself.

### 2.4.1 Autocorrelation

There are different ways to measure the autocorrelation of a pulse. The technique described here measures the so-called interferometric autocorrelation (IAC). In Fig. 2.4 it is shown how this technique is realized experimentally. The pulse is sent into a Michelson interferometer and at the output there is an SHG-crystal and a photodiode which measures intensity of the frequency-doubled light. The signal on the photodiode can be written as

$$I_{PD}(\tau) \propto \int_{-\infty}^{\infty} |(E(t) + E(t-\tau))^2|^2 dt. \quad (2.54)$$

$\tau$  is the delay between the pulses. Examples for interferometric autocorrelations are shown in Fig. 2.5.

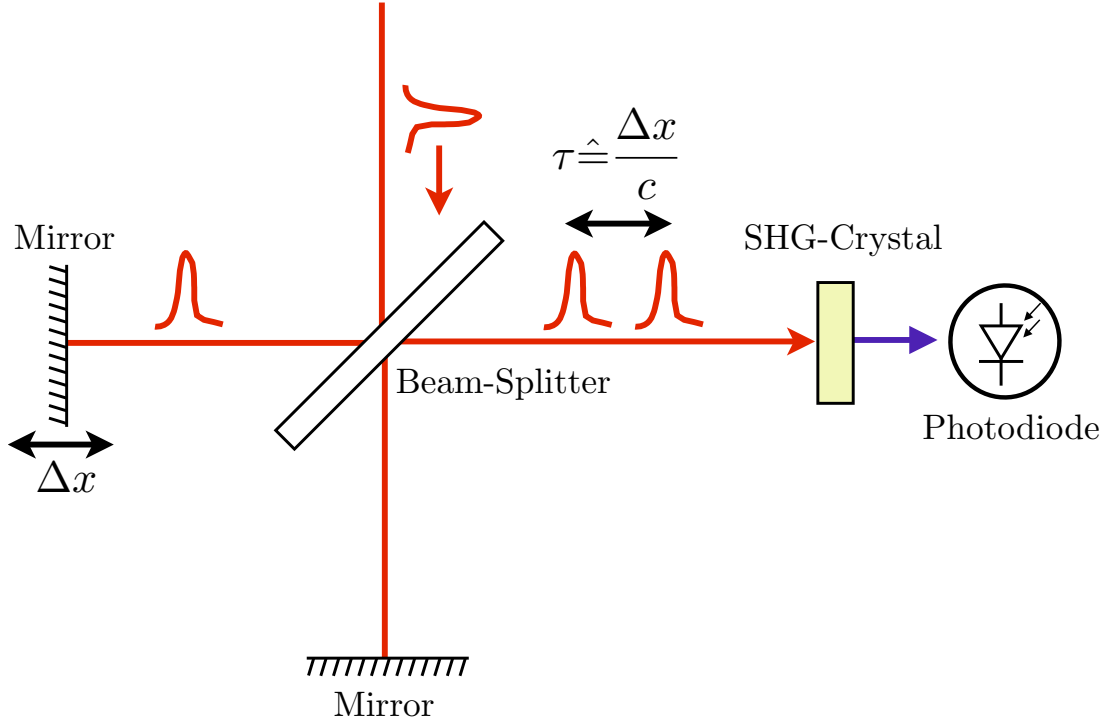


**Figure 2.4:** Interferometric Autocorrelation Setup: The beam splitter splits the pulse up into two replicas. One replica is delayed with respect to the other. Both replicas are sent through an SHG crystal. The photodiode detects the generated second harmonic.

So what exactly does the IAC measure? Clearly it contains information about the length of the pulse. For a gaussian pulse the FWHM of the IAC is by a factor  $\sqrt{2}$  larger than the FWHM of the pulse. It also includes some phase information. For a linearly chirped pulse the wings of the IAC do not have oscillations (the different frequencies in the leading and the trailing edge of the pulse do not cause interference fringes), but there is no way to measure the sign of the chirp. In general one can say that the more complicated a pulse is, the harder it is to characterize it from its IAC. So it is really worth it to build some better apparatus to measure ultrashort pulses, for example a SHG-FROG-setup.

## 2.4.2 FROG: Frequency-Resolved Optical Gating

The FROG-Setup is shown in Fig. 2.6. There are many different FROG-geometries [DeL96], here we choose a second-harmonic-generation FROG (SHG-FROG) because

## 2 Theoretical Background

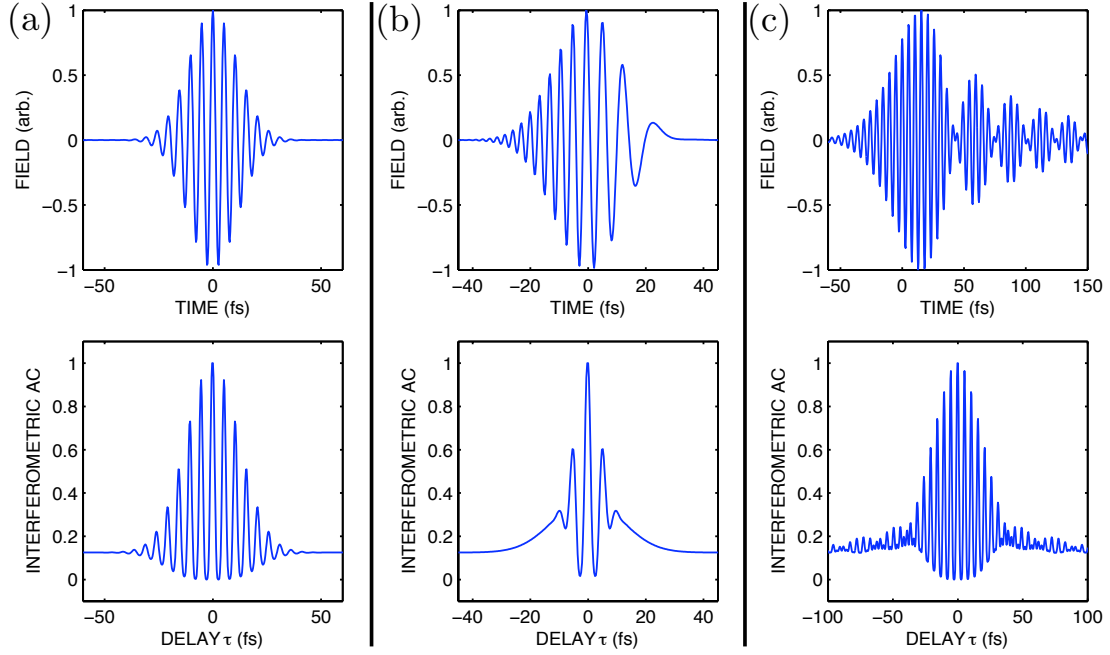


**Figure 2.5:** Pulses and their calculated interferometric autocorrelations. (a) A fourier-limited pulse. (b) A chirped pulse. (c) A pulse with third order phase distortion.

it is the most suitable to also measure pulses with low intensities<sup>‡</sup>. To convert the IAC setup into a SHG-FROG setup one has to do some simple modifications. There is one additional mirror to separate the two beams going into the SHG crystal. The beams are spatially overlapped inside the SHG crystal by an additional lens. The photodiode is replaced by an optical spectrometer that is able to measure the sum frequency of the incoming pulses. This apparatus measures the spectrogram (more precisely the auto-spectrogram) of the pulse, which is called FROG trace. A spectrogram is a picture that represents the spectral density versus time. One measures the FROG trace by scanning the delay line and by recording the corresponding spectra. Mathematically, the FROG trace is given by

$$I_{\text{SHG}}(\omega, \tau) = \left| \int_{-\infty}^{\infty} E(t)E(t - \tau) \exp(-i\omega t) dt \right|^2 \quad (2.55)$$

A measured FROG trace is shown in Fig. 2.7. Now one has to extract the complex-valued electric field from the FROG trace. Sadly, there is no known solution to analytically invert Eq. 2.55. But as this problem is known in the literature as the "2d phase-retrieval problem", there are many algorithms to retrieve the complex electric field. The software used in this thesis to retrieve pulses is FROG 3.2.2 from Femtosoftware Technologies, which uses an algorithm known as generalized projections [DeL94].

<sup>‡</sup>SHG-FROG uses the second-order nonlinearity, whereas all the other geometries are using third-order nonlinearity, which is much weaker

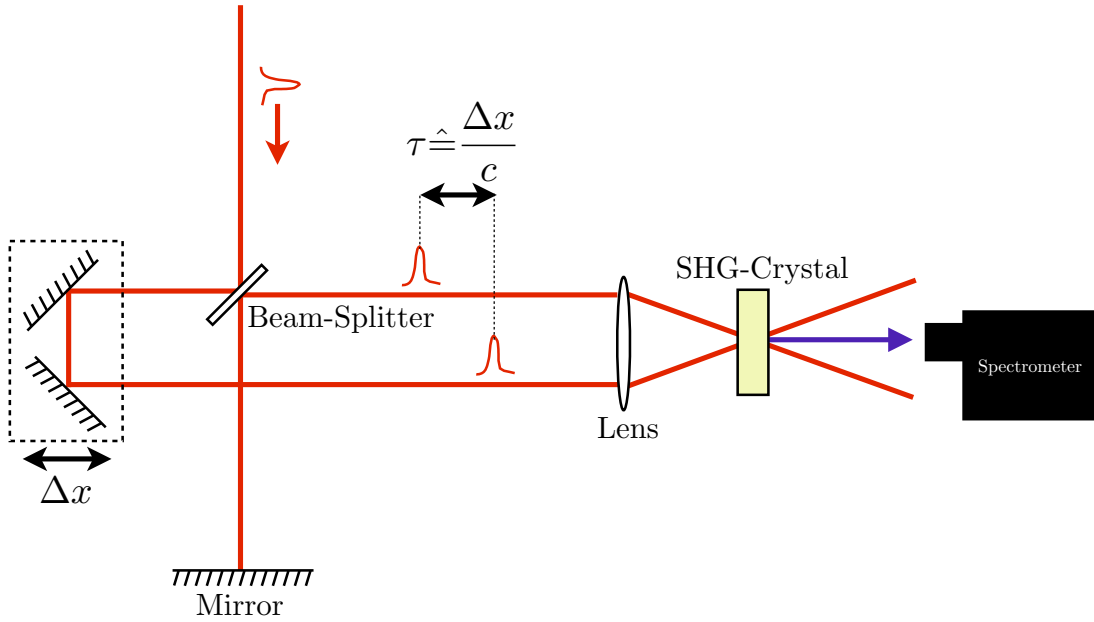


**Figure 2.6:** FROG setup: The beam splitter splits the pulse up into two replicas. One replica is delayed with respect to the other and displaced. The two beams are focused by a lens (or a spherical mirror). The focus, where the two beams spatially overlap, is in the center of a thin nonlinear crystal. Only the sum frequency is detected with the spectrometer.

The software calculates the complex electric field to which the FROG trace (the "retrieved" FROG trace) is as close as possible to the measured FROG trace. The FROG error, which is the root mean square difference between the FROG traces, indicates how large the difference is.

The SHG-FROG also has some ambiguities, but fortunately a lot less than IAC. First, the absolute phase can not be determined. As the arrival time of the pulses is not measured there is no information about the linear phase in the frequency domain (see Fig. 2.2). Second, the SHG-FROG trace is symmetrical with respect to delay, so there is an ambiguity with the direction of time. The retrieved pulse in time domain might as well be time-reversed.

An alternative to a FROG device might be the GRENOUILLE (Grating-eliminated no-nonsense observation of ultrafast incident laser e-fields) [Akt04, Gu04]. Technically, the GRENOUILLE is a much simpler device. It gets along without a delay line and without a spectrometer. The delay line, the beam splitter and the beam combining optics are replaced by one Fresnel prism. Instead of the thin nonlinear crystal and the spectrometer a thicker crystal and a CCD camera are used. Once the GRENOUILLE is built, the alignment is easier and the sensitivity is better compared to FROG. More details can be found in [Tre02].

## 2 Theoretical Background

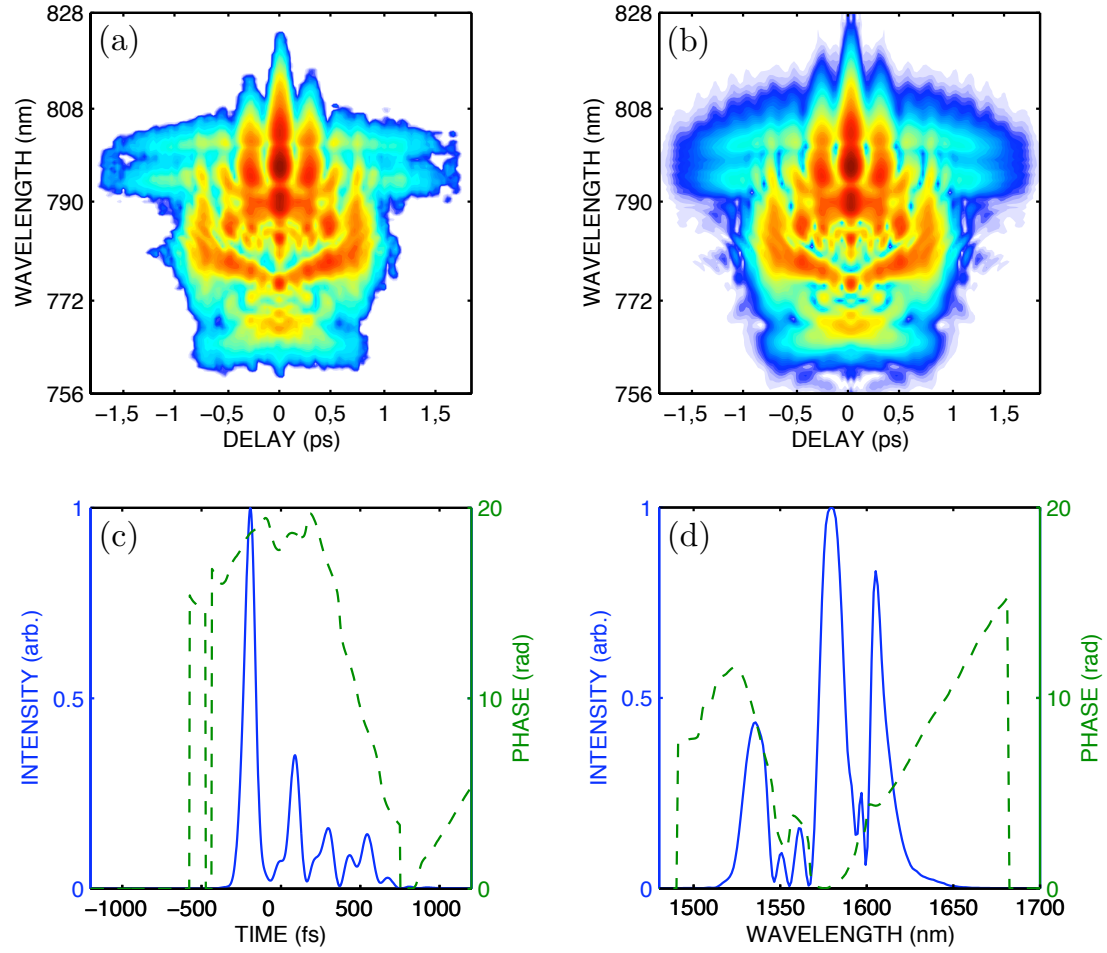


**Figure 2.7:** (a) A measured FROG trace of a rather complicated pulse. (b) The retrieved FROG trace. This trace was retrieved from (a) with the software FROG 3.2.2., the FROG error is 0.015. (c) The pulse corresponding to the retrieved FROG trace. The plot shows the normalized intensity (solid) and the phase (dashed). (d) The spectrum corresponding to the retrieved FROG trace. The plot shows the normalized intensity (solid) and the phase (dashed).

## CHAPTER 3

### Experimental Setup

This chapter describes the whole experimental setup, which consist of three major parts.

The core of the frequency comb is the Erbium-doped fiber laser. It generates the train of ultrashort pulses with a rate around 100 MHz and an average power of 10-20 mW. The length of the pulses is on the order of 100 fs, the optical spectrum is about 60 nm wide.

After the fiber laser follows an Erbium-doped fiber amplifier. It amplifies the pulse train to an average power of 250-300 mW, further shortens the pulses, and broadens the spectrum. The laser and the amplifier are shown in Fig. 3.1.

To generate an octave spanning supercontinuum, the pulses are coupled into a highly nonlinear fiber, which broadens the optical spectrum to range from  $1\ \mu\text{m}$  to more than  $2\ \mu\text{m}$ .

Additionally, we provide technical details of the FROG setup.

### 3.1 The Erbium-Fiber Laser

#### 3.1.1 Mode-Locking

The heart of the frequency comb is a mode-locked Erbium-fiber laser, which is built up as it is shown in Fig. 3.2. The important parts are the gain medium (Erbium-doped fiber), the pump diode, the ring resonator, and the mode-locking mechanism. The gain spectrum is broad enough, so that the laser is in principle able to generate short pulses around 100 fs. To really ensure the pulsed operation of the fiber laser a mode-locking mechanism is necessary [Ipp94, Hau91]. The term mode-locking comes from the description in frequency domain. The mode-locking makes sure that there is a fixed phase relation between all the amplified frequencies. In time domain that means that there are points of destructive and constructive interference, whereas the latter are the desired pulses.

There are many different mode-locking mechanisms [Ipp94]. The one that is used in this project is called polarization additive-pulse mode locking (P-APM). It uses the fact that due to the nonlinear refraction of the fiber, different intensities see a different index of refraction. For elliptically polarized radiation the consequence is polarization rotation. Fig. 3.3 illustrates how the P-APM mechanism works. A pulse with a strongly elliptic polarization is sent into a Kerr-medium. Dependent on the intensity

### 3 Experimental Setup

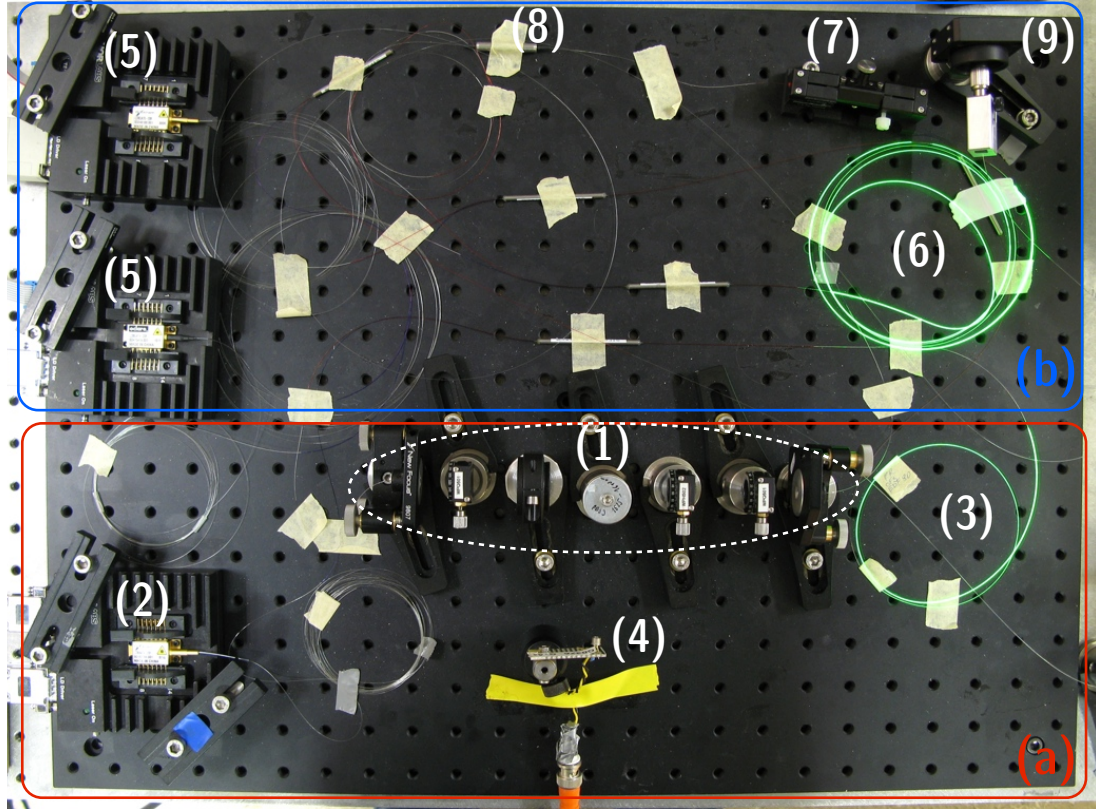


**Figure 3.1:** Experimental laser setup: (a) Erbium-fiber laser: (1) free-space path with mode-locking elements, (2) 600 mW pump diode, (3) Erbium-doped gain fiber, (4) monitoring photodiode. (b) Erbium-fiber amplifier: (5) 600 mW pump diodes, (6) Erbium-doped gain fiber, (7) polarization controller, (8) fiber isolator, (9) output.

there will be more or less polarization rotation. Combined with a polarizer which only transmits the rotated part (higher intensity) this acts as a "pulse-shortener". The mode-locking elements are located in the free-space path of the fiber laser. The polarizer is represented by a polarizing beam-cube and a Faraday-isolator. The quarter-wave plate (QWP) right behind the isolator makes the polarization elliptical, the other two waveplates change the polarization to maximize the transmission at pulsed operation. The mode-locking is self starting, meaning that the pulse builds up from initial cw-fluctuations.

#### 3.1.2 Repetition Rate and Total Dispersion

The repetition rate of the pulses is given by the optical-path length  $l_{\text{osc}}$  of the ring cavity by  $f_{\text{rep}} = c/l_{\text{osc}}$ . The cavity is built up from positive and negative GVD fiber, the pulse is periodically stretched and shortened. This kind of laser is a so-called stretched-pulse laser, which has been described in [Tam93].



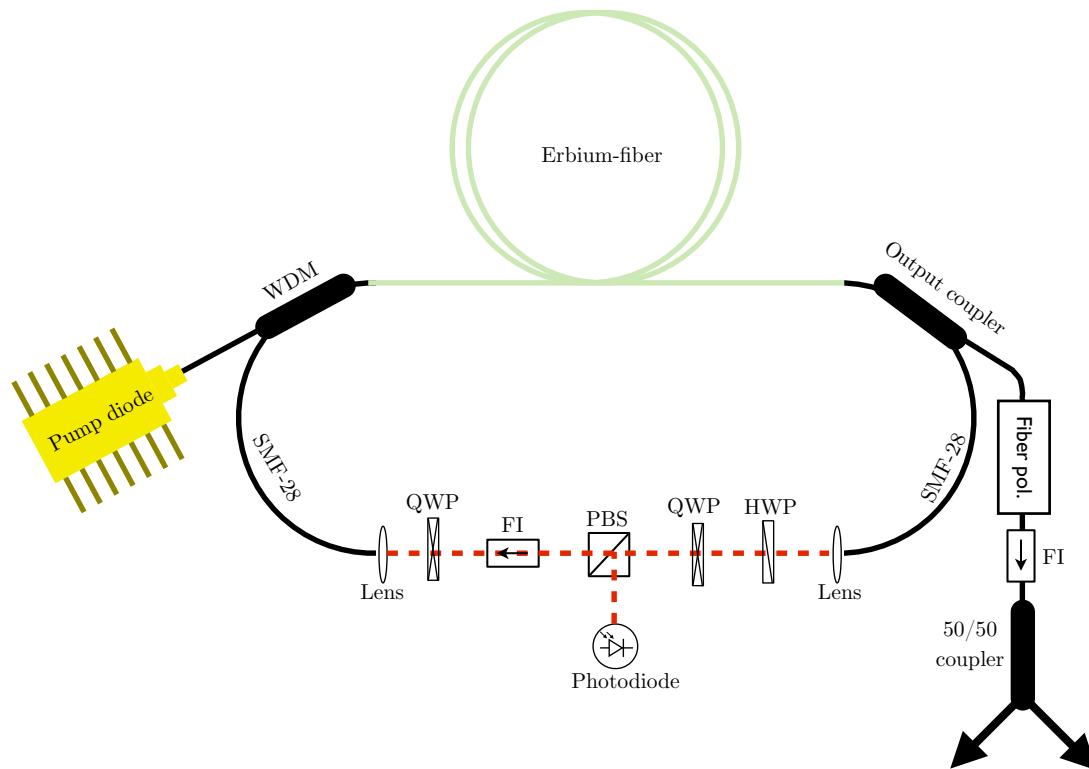


**Figure 3.2:** Erbium-fiber laser setup: QWP: quarter-wave plate, HWP: half-wave plate, PBS: polarizing beam splitter, FI: Faraday Isolator, WDM: wave division multiplexer.

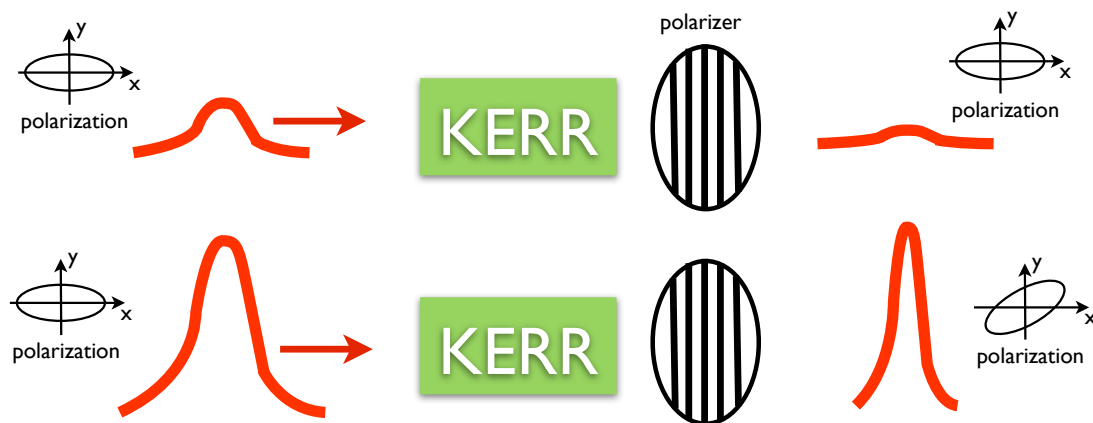


**Figure 3.3:** Scheme for polarization additive-pulse-mode locking (P-APM) [Ipp94]. The polarization of a weak pulse or cw-radiation is not effected by the nonlinearity, so it does not go through the polarizer. For a strong pulses, the peak is transmitted through the polarizer, and the wings are cut off.

### 3 Experimental Setup

The overall dispersion of the ring oscillator is dominated by the positive dispersion of the Erbium-doped gain fiber and the negative dispersion of the standard fiber (SMF-28), the optical components in the free-space path can be neglected. The overall dispersion should be close to zero for a minimum temporal pulse width [Tam94].

#### 3.1.3 Technical Details

The pump diode is a BOOKHAM LC96AA74-20R, which runs at 974 nm. The current for which mode-locking occurs is between 700 mA and 950 mA and provided by a WAVELENGTH ELECTRONICS MPL2500 driver. The pump power at 950 mA is 600 mW although there is a rather large splice loss (10-15%) at the splice from the diode to the wave division multiplexer (WDM). The reason is the very different fiber types. The polarization maintaining fiber from the pump diode has a different mode-field diameter and is made from different material than the SMF-28 from the WDM. The WDM is a SIFAM FFC-5C31P2210.

The diode is temperature stabilized to 25 °C by the integrated peltier element. The temperature controller is a homebuilt device.

The length of the gain fiber (OFS-EDF80) is 50 cm, the length of the standard fiber (Corning SMF-28) is 107 cm. The length of the free-space path is 19.5 cm. For coupling in and out of the fiber two fiber coupled collimation lenses are used (PHOTOP KFCL-A-250S-1550-Y-200-C-N). The corresponding repetition rate is 108 MHz. This could be easily adjusted to 100 MHz if necessary.

The light is coupled out by a 85/15 coupler. After the coupler follows a fiber polarizer (Thorlabs PLC-900) and a polarization dependent fiber isolator (OZ OPTICS FOI-21-11-1550-9/125-S-50-XX-0.25-1-40). The reason for not using polarization independent isolators is that they have a much higher polarization mode dispersion.

After the isolator the light is split up by a 50/50 fiber coupler. One port is going to the amplifier, the other port can be used for monitoring or could e.g. be used to seed another amplifier.

The 85/15 output coupler is placed right after the gain fiber where the pulses have a positive chirp. This chirp is compensated by an output lead of SMF-28 fiber. The shortest pulses are found after 175 cm of compensation fiber and are shown in Fig. 3.5. The pulse train has an average power of 16 mW.

The wave plates in the free-space path are telecom zero-order wave plates (Thorlabs WPQ501 and WPH501), the cube is a standard 3mm PBS. The isolator is a ISOWAVE mini single stage isolator. For monitoring the repetition rate a photo diode (InGaAs) with a resistor in parallel is placed next to the beamcube.

#### 3.1.4 Practical Mode-Locking Concerns

After assembling an Erbium-doped fiber laser the mode-locking has to be done by basically rotating the three wave plates into the right position. For our setup, the strategy to mode-lock the laser in the beginning was the following.

We turned up the pump diode to full power (950 mA). With our setup it was easier to achieve mode-locking at higher pump powers. In the beginning the laser was emitting cw-light. The wavelength of the output light was monitored with an optical spectrum analyzer. It was at around 1533 nm and 1556 nm or both, depending on the position of the wave plates. The signal from the monitoring photodiode was observed with a spectrum analyzer (Fig. 3.4). There we could observe a peak at the repetition rate and some smaller side-peaks at a distance of a couple of 100 kHz (dependent on the position of the wave-plates). At certain wave plate settings fringes could be observed around the  $f_{\text{rep}}$ -peak, this is shown in Fig. 3.4(b). With that wave plate setting, the laser was already close to mode-locking. With careful further adjustment of the wave-plates mode-locking could be achieved.

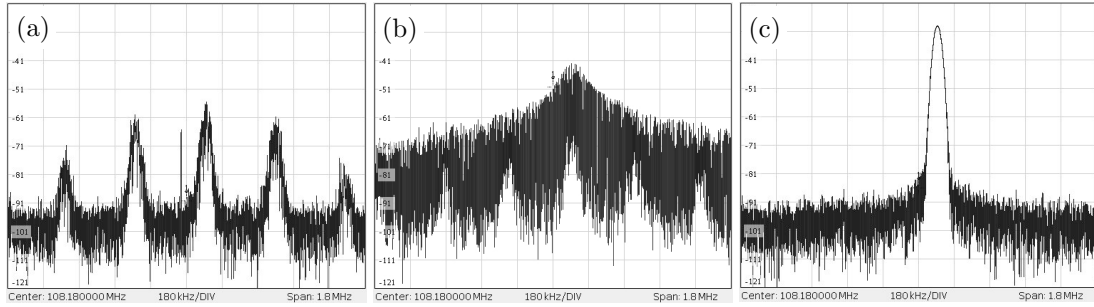


**Figure 3.4:** Measured spectra from the monitoring photodiode signal. Center: 108 MHz, Span 1.8 MHz, horizontal scale: 180 kHz/div, vertical scale: 10 dB/div Bandwidth 30 kHz. (a) far away from mode-locking, (b) closer to mode-locking, (c) The laser is mode-locked, the peak at 108 MHz represents the repetition rate of the pulses. The corresponding pulse and optical spectrum are shown in Fig. 3.5

## 3.2 The Erbium-Fiber Amplifier

The small output power of the fiber laser and especially the goal to create a supercontinuum make it necessary to add an amplifier. For the creation of a supercontinuum in a highly nonlinear fiber (HNLF), as it will be described in the next section, it is necessary to have a short, stable, and intense pulse.

In principle the design of a fiber amplifier is easy. It is shown in Fig. 3.6. Such amplifiers are widely used for long range telecommunication systems. The amplification with this kind of fiber amplifier can be higher than 10 dB [Des87]. The difficulty arises from the amplification of an ultrashort pulse without temporarily broadening or even destroying the pulse.

On the one hand, as the pulse becomes more and more amplified, nonlinear effects, especially SPM start to play an important role. The effect broadens the spectrum but can also destroy the stable shape of the pulse. On the other hand, as the gain

### 3 Experimental Setup

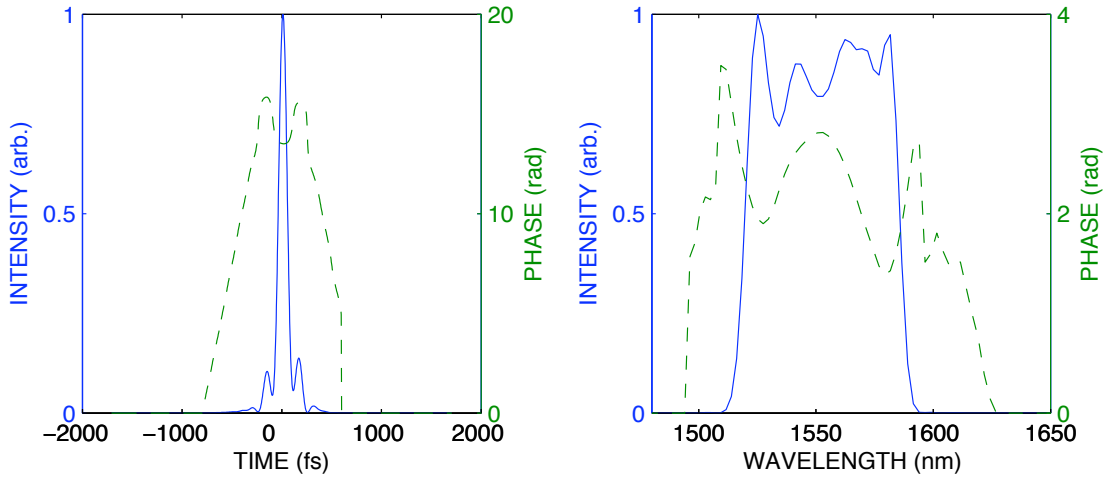


**Figure 3.5:** Output pulse of the fiber laser characterized with SHG-FROG. The plot shows the normalized intensity (solid) and the phase (dashed). The pulse is measured after a 175 cm long output lead of SMF-28 fiber. This fiber compensates for the positive chirp the pulse exhibits after the Erbium-doped fiber. The temporal FWHM is 96 fs, the spectrum FWHM is 66 nm.

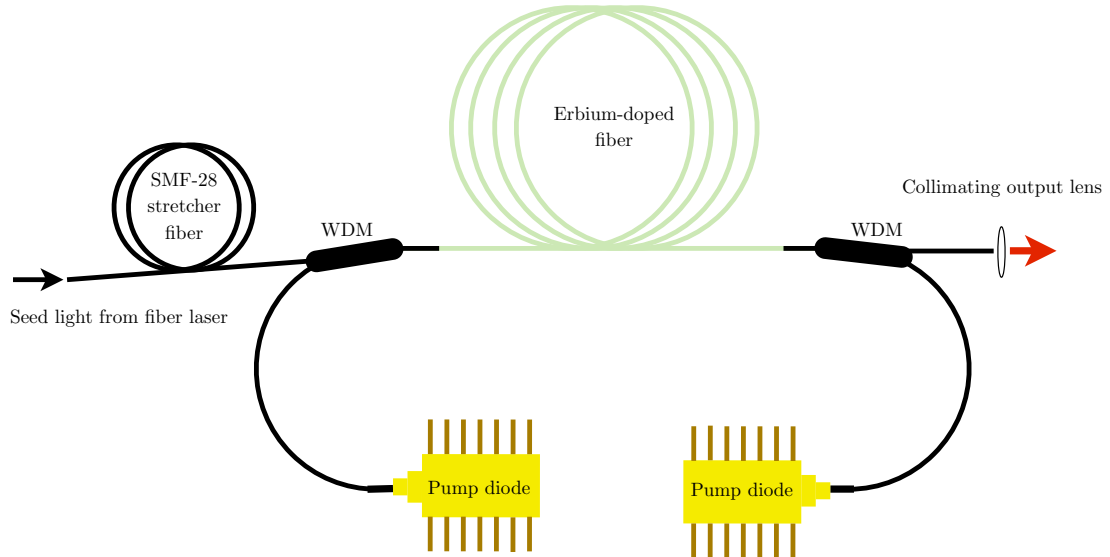


**Figure 3.6:** Experimental setup of the Erbium-fiber amplifier. WDM: wave division multiplexer. The seed pulses from the Erbium-fiber laser (Fig. 3.2) are pre-stretched inside the SMF-28 fiber and afterwards amplified and compressed inside the Erbium-doped fiber.

spectrum of the Erbium-doped fiber is narrower than the spectrum of the input pulse, gain-narrowing occurs. Dispersion also plays an important role, it temporally broadens the pulse, or can lead to solitonic effects, in case of an anomalous dispersion fiber.

One solution to address those problems is the so-called "stretched pulse amplifier" [Tau04b, Tau03, Tau04a]. The idea is to stretch the pulse in a standard fiber with anomalous dispersion so that it goes into the gain fiber with negative chirp. The gain fiber has normal dispersion, so that the pulse is re-compressed and amplified after the gain fiber. This scheme reduces the nonlinear effects, because the pulse is stretched and so the peak intensity is lower. It has also been shown in [Tam96] that in a normal dispersion fiber amplifier (NDFA) a pulse with parabolic shape evolves and further that those pulses can resist optical wave breaking.

Fig. 3.7 shows measurement of output pulses for different length of stretcher fiber. With a long stretcher fiber the pulse has a large negative chirp as it goes into the amplifier. The output spectrum is narrower than the input spectrum (Fig. 3.5) due to gain narrowing and SPM. SPM is normally associated with spectral broadening but for pulses with a strong negative chirp it has been shown that SPM causes narrowing in the spectrum [Obe93]. With a stretcher fiber of  $l_s = 620$  cm a pulse spectrum with a FWHM of only 5 nm was measured.

With a shorter stretcher fiber the pulse has less negative chirp. The spectrum broadens inside the amplifier. The output pulse usually exhibits some amount of linear chirp (Fig. 3.7). It was not possible to totally remove the chirp from the output pulse by adjusting the stretcher fiber to various values. Even if the dispersion of the anomalous stretcher fiber (SMF-28:  $\beta_2 = -0.023$  ps<sup>2</sup>/m) and the dispersion of the Erbium-doped gain fiber (OFS EDF-80:  $\beta_2 = 0.057$  ps<sup>2</sup>/m) cancel out, there was still a chirped pulse at the output.

To generate a short pulse and hence a high peak intensity, this chirp has to be compensated. There is the possibility to use a prism compressor [For84] or to compress the pulse in an anomalous dispersion fiber [Nic04]. The latter is known as soliton-effect compressor [Agr89].

#### 3.2.1 Soliton-Effect Compression in Anomalous Dispersion Fiber

Higher order solitons have a periodic evolution pattern (Fig. 2.3). This kind of compression uses the fact that solitons go through an initial narrowing phase. If the compression fiber is chosen in the right length, the compression factor can be on the order of the soliton order  $N$ .

The disadvantage of this method is that the pulse develops wings where part of the energy is contained. The physical origin of this is that in the initial narrowing phase the evolution is dominated by SPM. The phase that comes from SPM has a gaussian shape, leading to a chirp that is only linear in the center of the pulse. The result of this is that only the central part of the pulse is compressed by the GVD.

Finding the right length of compression fiber can either be done by simulation, or just by splicing a long fiber at the output of the amplifier and cutting it piece by

### 3 Experimental Setup

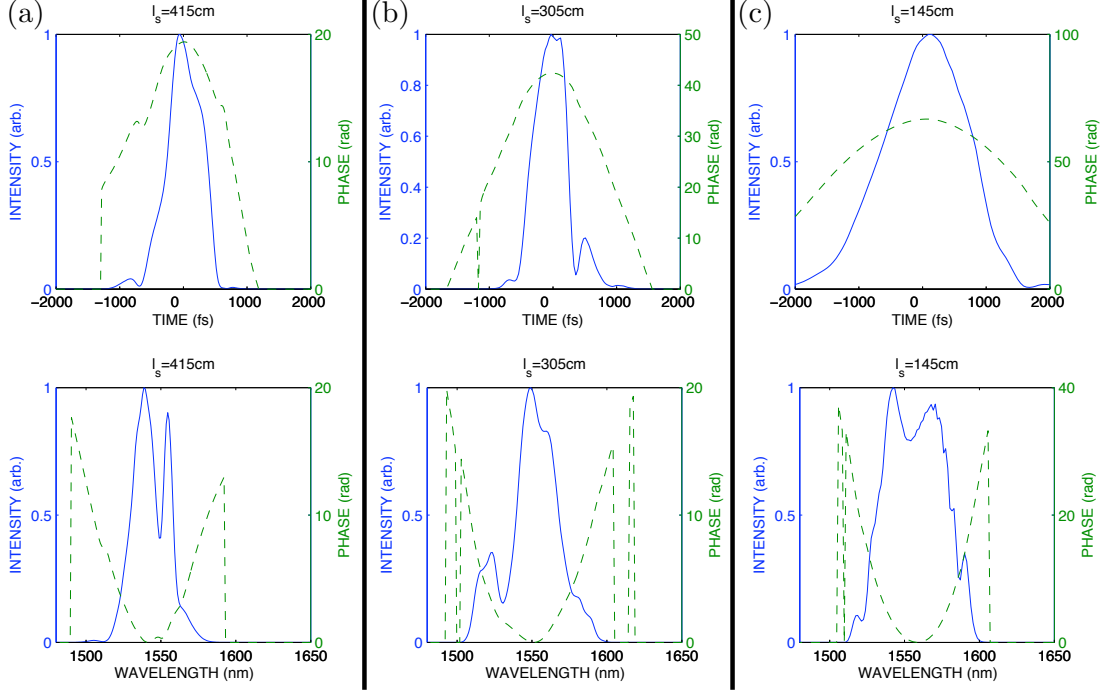


**Figure 3.7:** Output pulses and spectra characterized after the amplifier with SHG-FROG for different length of stretcher fiber  $l_s$ . The plot shows the normalized intensities (solid) and the phases (dashed). (a)  $l_s = 415$  cm, (b)  $l_s = 305$  cm, (c)  $l_s = 145$  cm. The pumps were both running with a current of 950 mA. The length of the output lead was 18 cm, the length of the gain fiber 160 cm. Those pulses have a linear chirp that can be compensated with additional fiber at the output or with a prism compressor.

piece. As the fiber parameters are usually not precisely known, and the measurement of the pulse right after the amplifier might also have some errors, the right fiber length was found by trial and error. Fig. 3.8 shows that the strongly chirped output pulse from the amplifier with  $t_{\text{FWHM}} = 680$  fs was compressed to a short intense pulse with  $t_{\text{FWHM}} = 45$  fs by using 100 cm of SMF-28 fiber. The simulation predicts the best compression after 80 cm.

#### 3.2.2 Prism Compressor

Another possibility to compress the pulse is to use a prism compressor [Zha99]. In App. B calculations for SF-10 prisms are presented. The prism compressor was not implemented in the experiment, because the dispersion that could have been achieved with reasonable prism distance and reasonable angle of incidence was not high enough to compensate for the chirp of  $400 \text{ fs}^2/\text{cm}$ . Also one loses power because of reflections.

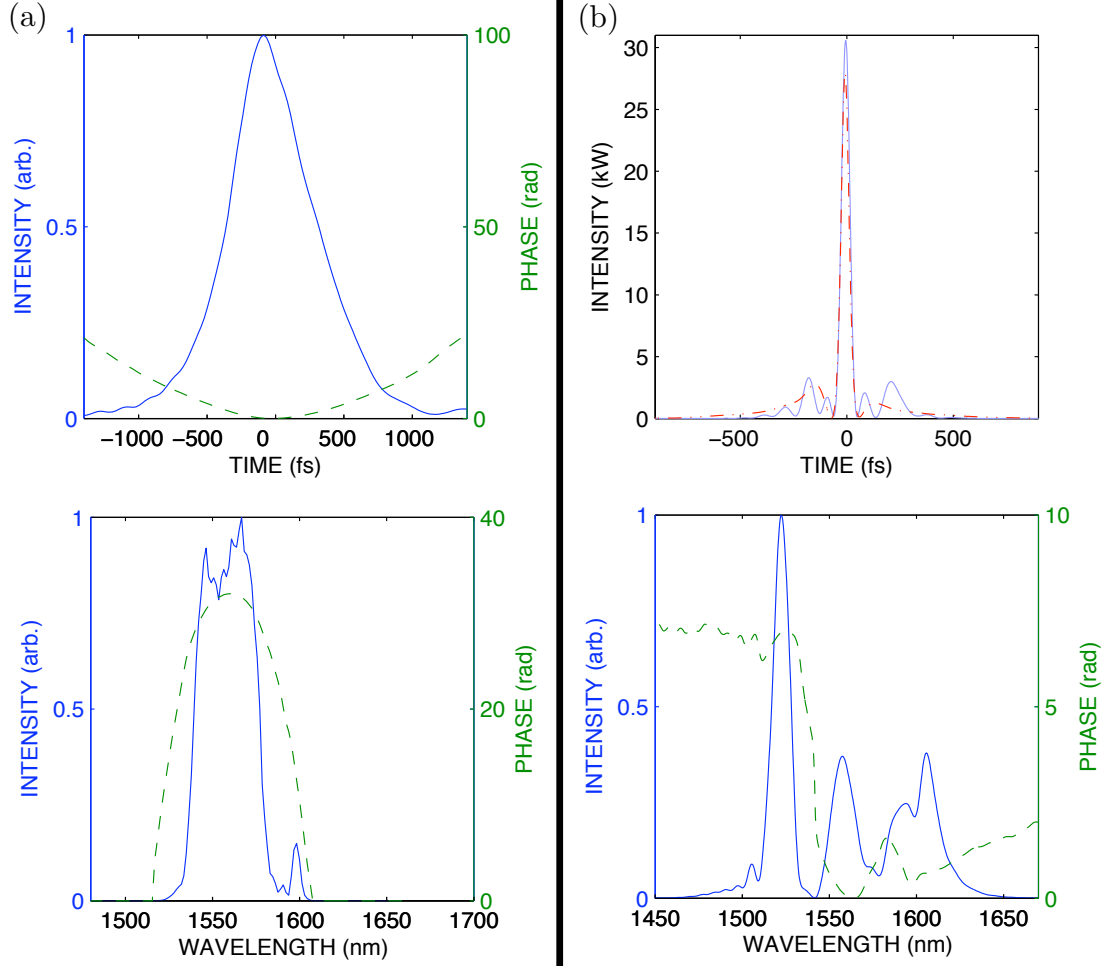


**Figure 3.8:** (a) Intensity and spectrum of the pulse characterized after a 75 cm long SMF-28 output lead. The plot shows the normalized intensity (solid) and the phase (dashed). The pulse has a FWHM of  $t_{\text{FWHM}} = 680$  fs. This measurement was done with a stretcher fiber of  $l_s = 255$  cm and a gain fiber of 160 cm. The pulse has a strong positive chirp of  $400 \text{ fs}^2/\text{cm}$ . (b) The measured (solid) compressed pulse after a 175 cm long output lead of SMF-28 fiber. The FWHM is 45 fs, 66% of energy is contained in the center-peak, the rest is in the wings. The simulation (dash dotted) shows good agreement, although the simulation predicts the shown pulse after 155 cm of output fiber. This discrepancy might come from the fact that the nonlinearity coefficient  $\gamma$  for the SMF-28 fiber was not precisely known and chosen to be  $1/\text{W/km}$ . The measured spectrum of the output pulse clearly shows further spectral broadening due to SPM.

#### 3.2.3 Technical Details

The pump diodes are BOOKHAM LC96AA74-20R and BOOKHAM LC96AA76-20R which are running at 974 nm and 976 nm. The advantage of two different colors is that the injection into the other diode is less likely [Adl07]. The diodes are driven by two WAVELENGTH ELECTRONICS MPL2500 and are temperature stabilized to 25 °C with a homebuilt device. The pump light is coupled into the gain fiber with two WDM (SIFAM FFC-5C31P2210). The length of the gain fiber (OFS-EDF80) is 160 cm for which a maximum output power of up to 300 mW could be found.

### 3.3 Supercontinuum Generation

By coupling a short intense pulse (Fig. 3.8(b)) into a highly nonlinear fiber (HNLF) the spectrum can be broadened. The goal is a spectrum that spans more than a factor of two, a so-called supercontinuum.

The highly nonlinear fiber (HNDS1614AB-9-2-2-1) that is used in this project is manufactured by Sumitomo Electric. This fiber has an extremely high nonlinear coefficient ( $\gamma = 30 \text{ /W/km}$ ) and a zero dispersion wavelength that is shifted to  $1.545 \mu\text{m}$ , a wavelength close to the center wavelength of the pulse.

The strong spectral broadening can not be explained with SPM alone, other effects such as the break up of the pulse into solitons, and four-wave mixing are involved [Hus02, Tau04a]. Fig. 3.9 shows a result of the simulation of the spectral broadening inside the HNLF. The input pulse for this simulation is the pulse from Fig. 3.8(b). The simulation was done by numerically solving the propagation equation (Eq. 2.49) with the split-step Fourier method. For that purpose the Matlab code from App. A was used.

#### 3.3.1 Coupling the Pulses into the Highly Nonlinear Fiber

The HNLF has a very small mode-field diameter (MFD) compared to standard fibers. The transverse mode of the incoming laser beam has to be matched to the mode of the HNLF to get a reasonable good coupling efficiency.

In the experimental setup (Fig. 3.1), the output beam from the amplifier, coming out of the SMF-28 compression fiber, is collimated with an aspheric lens ( $f=8.0 \text{ mm}$ ,  $\text{NA}=0.5$ ). The SMF-28 fiber has a MFD of  $10.4 \mu\text{m}$ . The HNLF (SUMITOMO HNDS1614AB-9-2-2-1) has an approximate MFD of  $3.3 \mu\text{m}$ . This number was calculated from effective area  $A_{\text{eff}} = 8.6 \mu\text{m}^2$  given in the data sheet with Eq. 2.21. To couple the beam into the HNLF an aspheric lens ( $f=2.75 \text{ mm}$ ,  $\text{NA}=0.55$ ) is used. This lens combination leads to a beam diameter of  $3.57 \mu\text{m}$  at the fiber core. The best coupling efficiency that has been achieved with this setup was about 75%.

Another possibility is to splice the HNLF directly onto the SMF-28 output lead of the amplifier. For this setup a so-called mode-field adapter (MFA) would be necessary. The MFA can be produced by thermal core expansion. The thermal core expansion



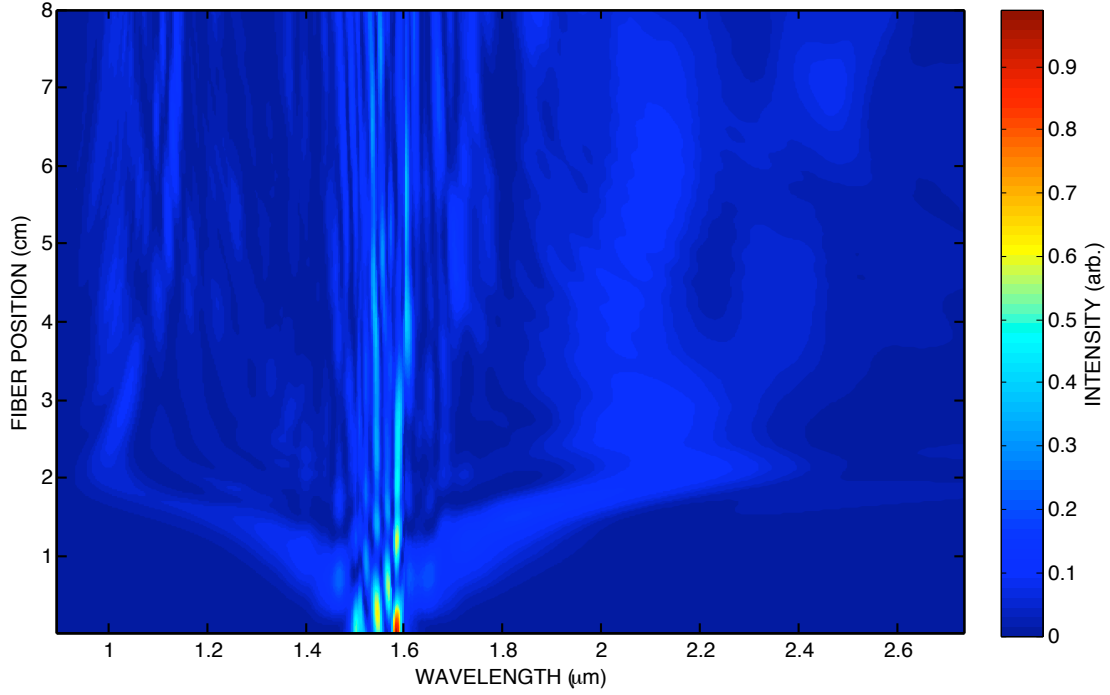


**Figure 3.9:** Result of a simulation of the spectral broadening inside an 8 cm long HNLF (SUMITOMO HNDS1614AB-9-2-2-1). The relevant fiber parameters are:  $\beta_2 = -1.28 \cdot 10^{-28} \text{ s}^2/\text{m}$ ,  $\beta_3 = 3.11 \cdot 10^{-41} \text{ s}^3/\text{m}$ ,  $\gamma = 30 \cdot 10^{-3} \text{ /W/m}$ . The simulation was done with the input pulse from Fig. 3.8(b) with a pulse energy of 1.39 nJ which corresponds to a peak intensity of 19 kW and an average power of 150mW.

can in principal be performed with the Vytran fusion fiber splicer FFS-2000 that has been used in this work. The idea is to thermally expand the core of the HNLF fiber to match the MFD to the SMF-28 fiber [Wan09]. With this method the coupling losses could be further decreased.

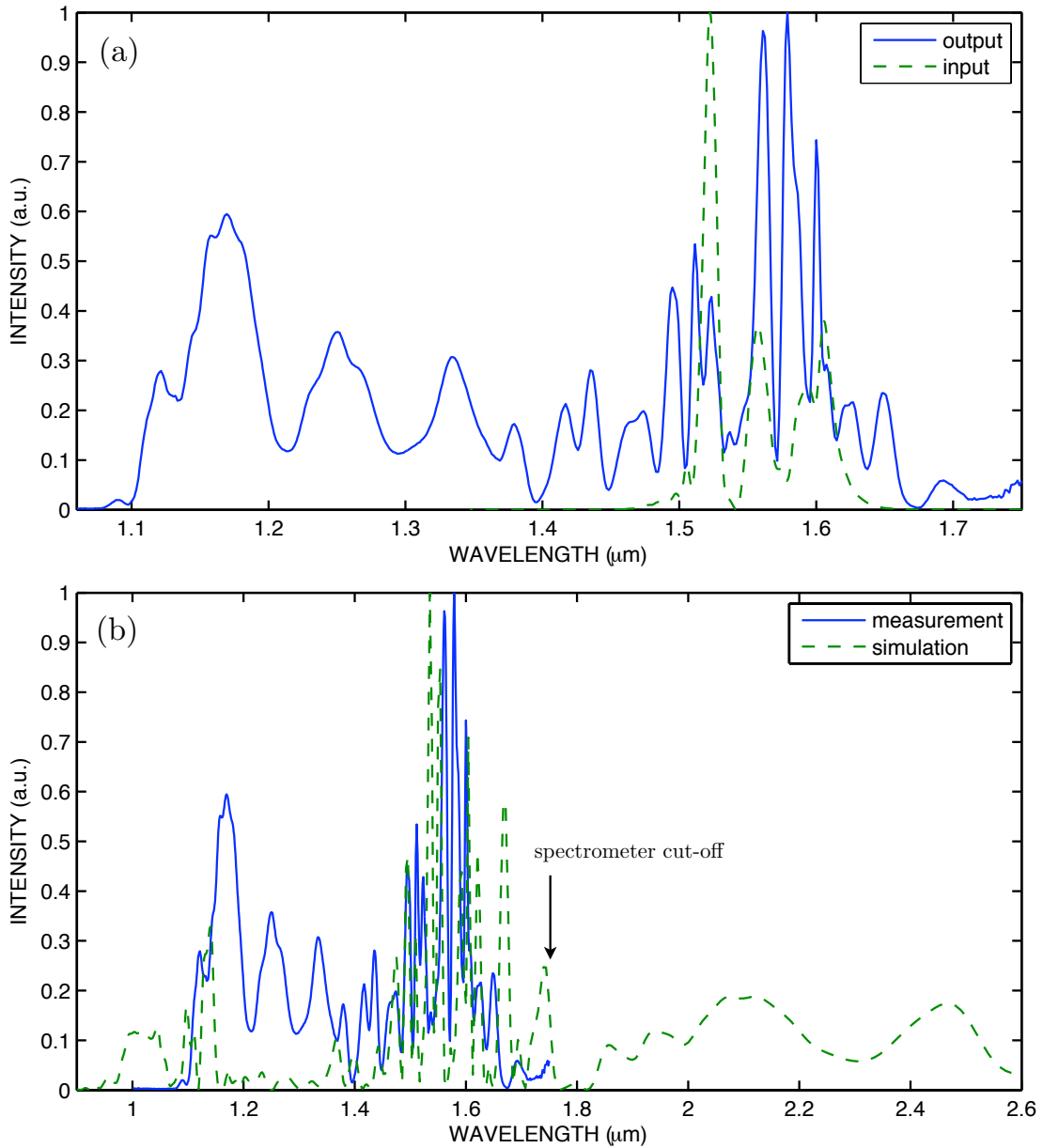
#### 3.3.2 Experimental Results

Fig. 3.10 shows the measured spectrum after 7 cm of HNLF (SUMITOMO HNDS1614AB-9-2-2-1). The average power after the HNLF is 155 mW which corresponds to a coupling efficiency of 66%.

To measure the spectrum, a fiber coupled optical spectrum analyser was used. The optical spectrum analyser can measure up to a wavelength of  $1.75 \mu\text{m}$ . The beam was collimated after the HNLF and coupled into 2 m of SMF-28 fiber that was connected to the optical spectrum analyser. The exact shape of the measured spectrum was dependent on the coupling into the SMF-28 fiber. The coupling was optimized to have as much amplitude as possible in the lower wavelength end of the spectrum.

It has also been investigated how the length of the HNLF effects the output spec-

### 3 Experimental Setup



**Figure 3.10:** Supercontinuum generation in a HNLF. The pulse from Fig. 3.8(b) was coupled into 7 cm of HNLF (SUMITOMO HNDS1614AB-9-2-2-1) with an average power of 155mW. After the HNLF, the beam was coupled into a SMF-28 fiber and the spectrum was measured with a fiber coupled ANDOR optical spectrum analyser, which can measure up to a wavelength of 1.75  $\mu\text{m}$ . (a) shows the spectrum before and after the HNLF. (b) shows the measured spectrum and the corresponding result of the simulation.

trum. The output spectra, that have been measured with several length of highly non-linear fibers from 10 cm down to 2.5 cm, did not show a significant qualitative difference. This behavior can also be seen in the result of the simulation in Fig. 3.9.

Clearly, the result of the simulation and the measured spectrum in Fig. 3.10 do not agree very well. That can have many reasons. It has been mentioned further above, that the measurement of the spectrum is only qualitatively right. This could explain why the distribution of the amplitude differs from the measurement to the result of the simulation. Another reason for the difference is the polarization of the input pulse. The simulation treats the electric field of the pulse as a scalar field and completely neglects the polarization. In the experiment, it could be seen that the spectrum after the HNLF is strongly dependent on the polarization of the input pulse. To measure the spectrum shown in Fig. 3.10 a quarter-wave plate and a half-wave plate were placed prior the HNLF. The polarization of the beam was optimized for maximum spectral broadening. Other uncertainties are the fiber parameters. Perhaps a better agreement could be achieved by slightly adjusting the fiber parameters for the simulation.

## 3.4 FROG Setup

The SHG-FROG-SETUP is shown in Fig. 3.11. There is an iris at the entrance which is convenient for guiding the beam into the device at the right height, and also for attenuating the beam if necessary. In the center there is a pellicle beamsplitter (Thorlabs BP245B3), which is used to split up the beam. The reason why there is no standard beamsplitter is that one wants to have as little dispersion as possible. The mirror in one arm (all mirrors in this setup are gold mirrors) just sends the beam back at constant height. The mirror in the other arm displaces the beam vertically by 23 mm and also sends it back onto the beamsplitter. This mirror is mounted on a motorized translation stage (Thorlabs MT1/M-Z8), which is operated by a Thorlabs TDC001 controller. For the translation stage it is important that the range and the resolution is large enough. For this work the longest pulses that occurred needed a range of more than 3 ps (Fig. 2.7) which corresponds to  $450\mu\text{m}^*$ . The smallest resolution used in this work was on the order of  $20\text{ fs} \hat{=} 3\mu\text{m}$ .

A two inch mirror is used as a folding mirror and a spherical mirror ( $f=200\text{ mm}$ ) focuses the beams into the nonlinear crystal. The nonlinear crystal (Cstech BBO,  $L = 100\mu\text{m}$ ,  $B \times H = 5 \times 5\text{ mm}$ , phase-matched for  $1550\text{ nm}$ ) is mounted on a rotation mount. To achieve uniform phase matching for the whole bandwidth of the pulse, it is necessary to use a very thin crystal. On the other hand the second-harmonic conversion efficiency scales with the square of the crystal length. The crystal used is a good compromise, it is thick enough to measure pulses with a couple of mW. The phase-matching bandwidth is huge with  $\delta\lambda = 10.57\mu\text{m}$ , so it is quite uniform around the center wavelength.

---

\*due to the folding of the path it is half the value of  $3\text{ ps} \cdot c$

### 3 Experimental Setup

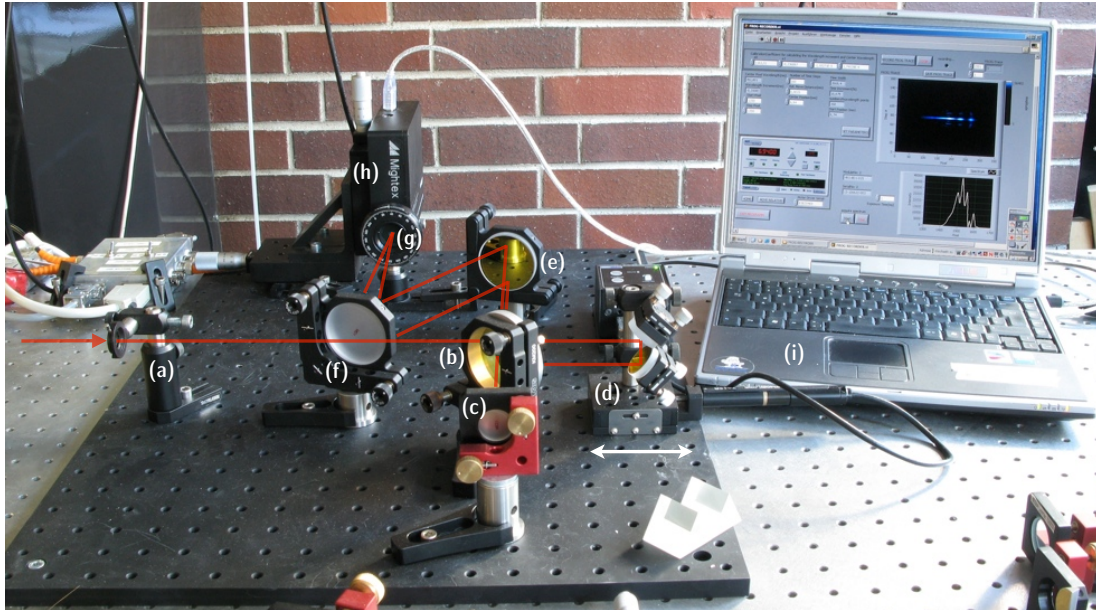


**Figure 3.11:** SHG-FROG setup: (a) Iris, (b) Pellicle beam splitter, (c) Gold mirror, (d) Delay line: a motorized translation stage with two gold mirrors that displace the beam vertically. (e) Folding mirror, (f) Spherical mirror, (g) BBO crystal, (h) Spectrometer, (i) a laptop with a Labview software that is connected to the spectrometer and the motorized translation stage via USB port.

After the SHG-crystal there is a spectrometer (Mightex HRS-BD1-025) that is mounted on a two dimensional translation stage to make the alignment easier.

For building the FROG setup, it is important that the beams spatially overlap inside the crystal. The beam that is coming from the delay should not change its position while moving the translation stage. If the spatial overlap is good enough, it is useful to place a photodiode right after the SHG-crystal, scan the delay line, and try to temporarily overlap the pulses by looking for an increasing signal on the photodiode. If that is done one can put the spectrometer in and try to measure the spectrum. It is important to make sure that the measured spectrum is the spectrum of the sum of the two beams, and not the frequency doubled spectrum of one single beam. This is easily checked by blocking the one beam and then the other, the measured spectrum has to disappear in both cases.

To record a FROG trace a LabView program was designed. Both, the TDC001 controller and the Mightex spectrometer have a USB connector. With this software it is possible to adjust all the important parameters, and save the FROG trace in a file that is compatible with FROG 3.2.2.

## CHAPTER 4

### Conclusion and Outlook

This master thesis describes the construction of a mode-locked Erbium-fiber laser and an Erbium-fiber amplifier. We could show that the laser system produces ultrashort laser pulses with durations down to 45 fs, a repetition rate of 100 MHz and an average output power of more than 240 mW.

To accomplish a working laser system it was necessary to build a setup for the characterization of ultrashort laser pulses. For this purpose an SHG-FROG setup has been built, which is able to characterize the pulses from the mode-locked Erbium-fiber laser as well as the pulses from the Erbium-fiber amplifier. The construction of the FROG setup involved the assembling of the setup on the table and the programming of a software to record and save the measured data. The FROG setup is an indispensable tool for the optimization of the laser output.

Further, simulations of the propagation equation (nonlinear Schrödinger equation) were presented. On the one hand, the simulations were helpful for the understanding of pulse propagation in optical fibers. Especially chromatic dispersion, nonlinear effects and their interplay, leading to physical phenomena like solitons, can be investigated with the simulation. On the other hand, the possibility to take a characterized pulse and to let it propagate through various fibers (as long as the fiber parameters are known) was helpful for the understanding of the pulse compression after the amplifier.

The simulation also made it possible to investigate the spectral broadening of an ultrashort laser pulse in a highly nonlinear fiber. The results show that it is theoretically possible to create an octave spanning supercontinuum with the pulse from our laser system.

We have also tried to experimentally realize a supercontinuum and proof the existence by measuring the carrier-envelope offset frequency with a  $f$ - $2f$  interferometer. It has been investigated that the spectrum barely spans a factor of two, but it was not enough to detect a carrier-envelope offset frequency beat above the noise.

To continue this project several tasks have to be addressed. The supercontinuum generation has to be further optimized to reach an octave spanning spectrum with sufficient power to measure the carrier-envelope offset frequency. It will further be possible to lock the carrier-envelope offset frequency to desired values by control of the fiber laser pump current.

Additionally, for locking the repetition rate, the length of the ring resonator has to be controlled. This could be done by controlling the free-space path length. In most conventional systems, this is achieved by mounting one coupling lens onto a piezo

#### *4 Conclusion and Outlook*

crystal.

Once the laser system is stabilized, it will be applicable in our experiments. With a spectral range of about  $1\,\mu\text{m}$  to  $2\,\mu\text{m}$  the Erbium-fiber laser system is especially interesting for experiments that focus on the generation of  $\text{Cs}_2$  ground-state molecules [Dan08, Dan10]. For the four photon STIRAP transfer from the weakly bound Feshbach molecules to the molecules in the rovibrational ground state, four lasers with wavelengths between 1003 nm and 1351 nm are used. Those wavelengths are covered by an Erbium-fiber frequency comb.

To cover a different wavelength range it is on the one hand possible to extend the comb spectrum by generating second harmonics of the Erbium-fiber frequency comb [Wid99]. On the other hand, it would be possible to use a different gain fiber. Ytterbium-fiber combs have a center wavelength of 1064 nm and a spectral range from about 670 nm up to 1500 nm [Sch08].

## APPENDIX A

### Matlab Source Code: Simulation of the Nonlinear Schrödinger Equation

```
%Symmetrized split-step Fourier Method
%Simulation of the NLSE

clear all

cspeed=299792458 ; % speed of lighth m/s
lambda0=1550e-9 ; % center wavelength in m

%sumitomo HNLF parameters
D=0.1e-6 ; % dispersion s/m^2
D_slope=0.019e3 ; % disp. slope s/m^3
b2=-(D*lambda0^2)/2/pi/cspeed % beta-2 coefficient s^2/m
b3=(D_slope*lambda0^4)/... % beta-3 coeff. s^3/m
    4/pi^2/cspeed^2-lambda0/pi/cspeed*b2 % nonlinear coeff /W/m
y=30e-3;

dt=2e-15; %time vector spacing
df=1/dt; %frequency vector spacing
dw=2*pi*df; %angular frequency vector
L=2^nextpow2(4000); %vector length
t = (-L/2:1:L/2-1)*dt; %time vector
f = (-L/2:1:L/2-1)*-df/L; %frequency vector
w = 2*pi*f; %angular frequency vector

fabs=f+cspeed/lambda0;
lambda =cspeed./fabs*1e6; %wavelength vector
wabs=2*pi*f;

%input pulse field(aini) and spectrum(afini)
tfwhm = 80e-15;
peakp=10000 %peakpower in W
aini=sqrt(peakp)*sech(1/tfwhm*t);
afini=1/df/sqrt(2*pi)*fftshift(fft(aini));

fiberlength=0.07 ; % in m
h=0.0003; % step size in m
```

## *A Matlab Source Code: Simulation of the Nonlinear Schrödinger Equation*

```
iterations=3           % number of iterations
i=sqrt(-1);

figure(1)

%symmetrized split-step fourier method
a=aini;
for j = 1:1:fiberlength/h
    anew=a;
    for itcount=1:iterations

        %dispersion 1
        af0=1/df/sqrt(2*pi)*fftshift(fft(fftshift(a)));
        af1=af0.*exp((h/2)*(+i/2*b2*wabs.^2-i/6*b3*wabs.^3));
        a1=1/dt*sqrt(2*pi)*ifftshift(ifft(ifftshift(af1)));

        %nonlinearity
        atrapz=1/2*(a+anew);
        a2=exp((i*y*h*(atrapz.*conj(atrapz)))).*a1;

        %dispersion 2
        af2=1/df/sqrt(2*pi)*fftshift(fft(fftshift(a2)));
        af3=exp((h/2)*(+i/2*b2*wabs.^2-i/6*b3*wabs.^3)).*af2;
        a3=1/dt*sqrt(2*pi)*ifftshift(ifft(ifftshift(af3)));

        anew=a3;
    end
    a=anew;

    specpic(j,:)=1/df/sqrt(2*pi)*fftshift(fft(fftshift(a)));

    %plotting...
    lp=350;
    lm=350;
    plot(t(L/2-lm:L/2+lp),1/max(abs(a3).^2).*abs(a3(L/2-lm:L/2+lp)).^2,...
        t(L/2-lm:L/2+lp),1/max(abs(aini).^2).*abs(aini(L/2-lm:L/2+lp)).^2,...
        t(L/2-lm:L/2+lp),1/max(angle(a3))*angle(a3(L/2-lm:L/2+lp)), 'red')
    axis([min(t(L/2-lm:L/2+lp)) max(t(L/2-lm:L/2+lp)) 0 2])
    xlabel('TIME (s)')
    ylabel('INTENSITY (a.u.)')
    title('Puls in time domain')
    subplot(3,1,3)

    plot(f,1/max(abs(af3)).*abs(af3),f,1/max(abs(afini)).*abs(afini))
    xlabel('FREQUENCY (Hz)')
    ylabel('INTENSITY (a.u.)')
    title('Puls spectrum')
```



```

subplot(3,1,2)

lp=L/2;
lm=L/2-1;
lambda_plot=lambda(L/2-lm:L/2+lp);
plot(lambda_plot,1/max(abs(af3).^2).*abs(af3(L/2-lm:L/2+lp)).^2,...
      lambda_plot,1/max(abs(afini).^2).*abs(afini(L/2-lm:L/2+lp)).^2,...
      lambda_plot,1/max(angle(af3)).*angle(af3(L/2-lm:L/2+lp)),'red')
axis([min(0.8) max(2.6) 0 1.1])
xlabel('WAVELENGTH (\mum)')
ylabel('INTENSITY (a.u.)')
title('Puls spectrum')
subplot(3,1,1)

drawnow
end

lp=500;
lm=900;
figure(2)
contourf(lambda(L/2-lm:L/2+lp),...
          1:fiberlength/h,abs(specpic(:,L/2-lm:L/2+lp)),100,'LineStyle','none')
xlabel('WAVELENGTH (\mum)')
ylabel('FIBER POSITION (a.u.)')

figure(3)
lambda_plot=lambda(L/2-lm:L/2+lp);
plot(lambda_plot,1/max(abs(afini).^2).*abs(afini(L/2-lm:L/2+lp)).^2,...
      lambda_plot,1/max(abs(af3).^2).*abs(af3(L/2-lm:L/2+lp)).^2)
xlabel('WAVELENGTH (\mum)')
ylabel('INTENSITY (a.u.)')
title('Puls spectrum')

figure(4)
lp=200;
lm=200;
plot(t(L/2-lm:L/2+lp),abs(a3(L/2-lm:L/2+lp)).^2,...
      t(L/2-lm:L/2+lp),abs(aini(L/2-lm:L/2+lp)).^2)
ylabel('INTENSITY (W)')
title('Puls in time domain')

```



## APPENDIX B

### Calculation for SF-10 Prism Compressor

The following calculations were done to estimate the total group delay dispersion (GDD) of a pair of equilateral prisms made from SF-10 glass in terms of prism separation  $l$  and angle of incidence  $\phi$ . The analytic formula was taken from [Zha99]. The setup of the compressor is shown in Fig. B.1. The incident pulse is dispersed at the first prism and collimated with the second prism. The mirror sends the pulse back on the same path. Longer wavelengths have a shorter path-length through the compressor, so the compressor has an overall negative dispersion.

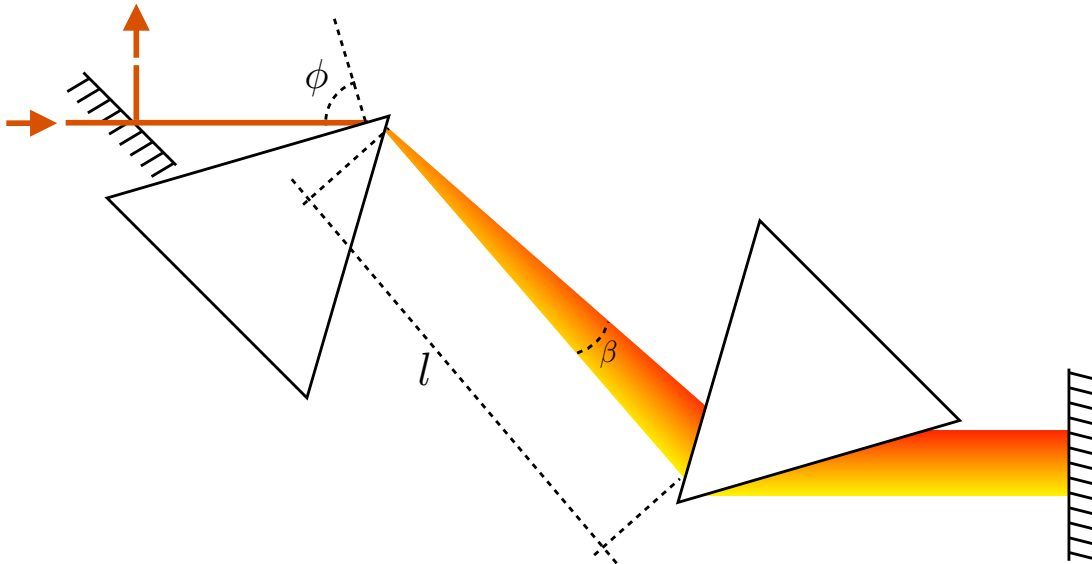


**Figure B.1:** Prism compressor setup. The prisms are made from SF-10 glass. The incoming beam is dispersed by the first prism and collimated by the second prism. The folding mirror sends the beam back on the same path. The pick-off mirror guides the beam out of the compressor.

The optical path length through the prism pair is given by

$$P = 2l \cdot \cos \beta \quad (\text{B.1})$$

where  $l$  is the prism separation.  $\beta$  is shown in Fig. B.1. By calculating the second derivative of the path length with respect to  $\lambda$  one gets the GDD. The derivatives of the index of refraction can be calculated from the Sellmair equation (Eq. 2.11). The

## B Calculation for SF-10 Prism Compressor

Sellmair coefficients for SF-10 are given in Table B.1. The results of the calculation are shown in Fig. B.2.

B1	B2	B3	C1	C2	C3
1.6162597	0.2592293	1.0776231	0.0127534	0.0581939	116.60768

Table B.1: Sellmair coefficients for SF-10 glass

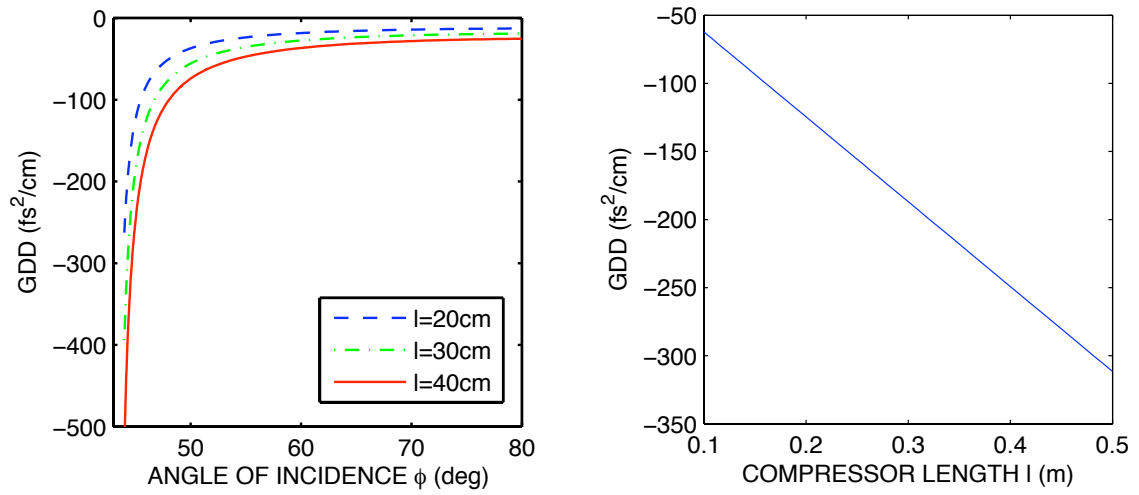


**Figure B.2:** left: GDD versus incidence angle  $\phi$  at different prism separation  $l$ . right: GDD versus prism separation at a 45° angle of incidence.

## References

- [Adl07] F. Adler, *Erbium-dotierte Femtosekunden-Faserlaser und Anwendungen*, Ph.D. thesis, Universität Konstanz (2007).
- [Agr89] G. P. Agrawal, *Non Linear Fiber Optics*, Academic Press, 1989.
- [Aik10] K. Aikawa, D. Akamatsu, M. Hayashi, K. Oasa, J. Kobayashi, P. Naidon, T. Kishimoto, M. Ueda, and S. Inouye, *Coherent Transfer of Photoassociated Molecules into the Rovibrational Ground State*, Phys. Rev. Lett. **105**, 203001 (2010).
- [Akt04] S. Akturk, M. Kimmel, R. Trebino, S. Naumov, E. Sorokin, and I. Sorokina, *Pulse-measurement challenges at 1.5 microns: several-cycle pulses and several-element devices*, in: *14th International Conference on Ultrafast Phenomena*, TuE21, Optical Society of America, 2004.
- [Ber98] K. Bergmann, H. Theuer, and B. W. Shore, *Coherent population transfer among quantum states of atoms and molecules*, Rev. Mod. Phys. **70**, 1003 (1998).
- [Biz03] S. Bize, S. A. Diddams, U. Tanaka, C. E. Tanner, W. H. Oskay, R. E. Drullinger, T. E. Parker, T. P. Heavner, S. R. Jefferts, L. Hollberg, W. M. Itano, and J. C. Bergquist, *Testing the Stability of Fundamental Constants with the  $^{199}\text{Hg}^+$  Single-Ion Optical Clock*, Phys. Rev. Lett. **90**, 150802 (2003).
- [Car09] L. D. Carr, D. DeMille, R. V. Krems, and J. Ye, *Cold and ultracold molecules: Science, technology and applications*, New. J. Phys. **11**, 055049 (2009).
- [Cho10] C. W. Chou, D. B. Hume, T. Rosenband, and D. J. Wineland, *Optical Clocks and Relativity*, Science **329**, 1630 (2010).
- [Dan08] J. G. Danzl, E. Haller, M. Gustavsson, M. J. Mark, R. Hart, N. Bouloufa, O. Dulieu, H. Ritsch, and H.-C. Nägerl, *Quantum gas of deeply bound ground state molecules*, Science **321**, 1062 (2008), published online 10 July 2008.
- [Dan10] J. G. Danzl, M. J. Mark, E. Haller, M. Gustavsson, R. Hart, J. Aldegunde, J. M. Hutson, and H.-C. Nägerl, *An ultracold high-density sample of rovibronic ground-state molecules in an optical lattice*, Nature Phys. (2010), advance online publication 21 Feb 2010, DOI: 10.1038/NPHYS1533.
- [DeL94] K. W. DeLong, *Pulse retrieval in frequency-resolved optical gating based on the method of generalized projections*, Optics Lett. **19**, 2152 (1994).

## References

- [DeL96] K. DeLong, D. Fittinghoff, and R. Trebino, *Practical issues in ultrashort-laser-pulse measurement using frequency-resolved optical gating*, Quantum Electronics, IEEE Journal of **32**, 1253 (1996).
- [Des87] E. Desurvire, J. R. Simpson, and P. C. Becker, *High-gain erbium-doped traveling-wave fiber amplifier*, Opt. Lett. **12**, 888 (1987).
- [Did00] S. A. Diddams, D. J. Jones, J. Ye, S. T. Cundiff, J. L. Hall, J. K. Ranka, R. S. Windeler, R. Holzwarth, T. Udem, and T. W. Hänsch, *Direct Link between Microwave and Optical Frequencies with a 300 THz Femtosecond Laser Comb*, Phys. Rev. Lett. **84**, 5102 (2000).
- [Did01] S. A. Diddams, T. Udem, J. C. Bergquist, E. A. Curtis, R. E. Drullinger, L. Hollberg, W. M. Itano, W. D. Lee, C. W. Oates, K. R. Vogel, and D. J. Wineland, *An Optical Clock Based on a Single Trapped  $^{199}\text{Hg}^+$  Ion*, Science **293**, 825 (2001).
- [For84] R. I. Fork, O. E. Martinez, and J. P. Gordon, *Negative dispersion using pairs of prisms*, Opt. Lett. **9**, 150 (1984).
- [Gór02] K. Góral, L. Santos, and M. Lewenstein, *Quantum phases of dipolar bosons in optical lattices*, Phys. Rev. Lett. **88**, 170406 (2002).
- [Gro61] E. Gross, *Structure of a quantized vortex in boson systems*, Il Nuovo Cimento (1955-1965) **20**, 454 (1961), 10.1007/BF02731494.
- [Gu04] X. Gu, S. Akturk, A. Shreenath, Q. Cao, and R. Trebino, *The Measurement of Ultrashort Light Pulses—Simple Devices, Complex Pulses*, Optical Review **11**, 141 (2004), 10.1007/s10-043-0041-8.
- [Hän06] T. W. Hänsch, *Nobel Lecture: Passion for precision*, Rev. Mod. Phys. **78**, 1297 (2006).
- [Hau91] H. A. Haus, J. G. Fujimoto, and E. P. Ippen, *Structures for additive pulse mode locking*, J. Opt. Soc. Am. B **8**, 2068 (1991).
- [Hol00] R. Holzwarth, T. Udem, T. W. Hänsch, J. C. Knight, W. J. Wadsworth, and P. S. J. Russell, *Optical Frequency Synthesizer for Precision Spectroscopy*, Phys. Rev. Lett. **85**, 2264 (2000).
- [Hus02] A. V. Husakou and J. Herrmann, *Supercontinuum generation, four-wave mixing, and fission of higher-order solitons in photonic-crystal fibers*, J. Opt. Soc. Am. B **19**, 2171 (2002).
- [Ipp94] E. P. Ippen, *Principles of passive mode locking*, Applied Physics B: Lasers and Optics **58**, 159 (1994).
- [Lan08] F. Lang, K. Winkler, C. Strauss, R. Grimm, and J. Hecker Denschlag, *Ultracold triplet molecules in the rovibrational ground state*, Phys. Rev. Lett. **101**, 133005 (2008).

- [Liu07] Y. Liu, J. E. Sharping, and M. T. Cicerone, *Numerical simulation of supercontinuum generation in GeO<sub>2</sub> doped fiber*, Proc. of SPIE **6698** (2007).
- [Mus05] G. Muslu and H. Erbay, *Higher-order split-step Fourier schemes for the generalized nonlinear Schroedinger equation*, Mathematics and Computers in Simulation **67**, 581 (2005).
- [Ni08] K.-K. Ni, S. Ospelkaus, M. H. G. de Miranda, A. Pe'er, B. Neyenhuis, J. J. Zirbel, S. Kotochigova, P. S. Julienne, D. S. Jin, and J. Ye, *A high phase-space-density gas of polar molecules*, Science **322**, 231 (2008).
- [Nic04] J. W. Nicholson, A. D. Yablon, P. S. Westbrook, K. S. Feder, and M. F. Yan, *High power, single mode, all-fiber source of femtosecond pulses at 1550 nm and its use in supercontinuum generation*, Opt. Express **12** (2004).
- [Nie00] M. Niering, R. Holzwarth, J. Reichert, P. Pokasov, T. Udem, M. Weitz, T. W. Hänsch, P. Lemonde, G. Santarelli, M. Abgrall, P. Laurent, C. Salomon, and A. Clairon, *Measurement of the Hydrogen 1S - 2S Transition Frequency by Phase Coherent Comparison with a Microwave Cesium Fountain Clock*, Phys. Rev. Lett. **84**, 5496 (2000).
- [Obe93] M. Oberthaler and R. A. Hopfel, *Special narrowing of ultrashort laser pulses by selfphase modulation in optical fibers*, Appl. Phys. Lett. **63**, 1017 (1993).
- [Ran00] J. K. Ranka, R. S. Windeler, and A. J. Stentz, *Visible continuum generation in air-silica microstructure optical fibers with anomalous dispersion at 800 nm*, Opt. Lett. **25**, 25 (2000).
- [Rei99] J. Reichert, R. Holzwarth, T. Udem, and T. W. Hänsch, *Measuring the frequency of light with mode-locked lasers*, Optics Communications **172**, 59 (1999).
- [Rei00] J. Reichert, M. Niering, R. Holzwarth, M. Weitz, T. Udem, and T. W. Hänsch, *Phase Coherent Vacuum-Ultraviolet to Radio Frequency Comparison with a Mode-Locked Laser*, Phys. Rev. Lett. **84**, 3232 (2000).
- [Ros08] T. Rosenband, D. B. Hume, P. O. Schmidt, C. W. Chou, A. Brusch, L. Lorini, W. H. Oskay, R. E. Drullinger, T. M. Fortier, J. E. Stalnaker, S. A. Diddams, W. C. Swann, N. R. Newbury, W. M. Itano, D. J. Wineland, and J. C. Bergquist, *Frequency Ratio of Al<sup>+</sup> and Hg<sup>+</sup> Single-Ion Optical Clocks; Metrology at the 17th Decimal Place*, Science **319**, 1808 (2008).
- [Sch96] H. Schnatz, B. Lipphardt, J. Helmcke, F. Riehle, and G. Zinner, *First Phase-Coherent Frequency Measurement of Visible Radiation*, Phys. Rev. Lett. **76**, 18 (1996).
- [Sch08] T. R. Schibli, I. Hartl, D. C. Yost, M. J. Martin, A. Marcinkevicius, M. E. Hermann, and J. Ye, *Optical frequency comb with submillihertz linewidth and more than 10 W average power*, Nat. Photonics **2**, 355 (2008).

## References

- [Tam93] K. Tamura, E. P. Ippen, H. A. Haus, and L. E. Nelson, *77-fs pulse generation from a stretched-pulse mode-locked all-fiber ring laser*, Opt. Lett. **18**, 1080 (1993).
- [Tam94] K. Tamura, L. E. Nelson, H. A. Haus, and E. P. Ippen, *Soliton versus non-soliton operation of fiber ring lasers*, Appl. Phys. Lett. **64** (1994).
- [Tam96] K. Tamura and M. Nakazawa, *Pulse compression by nonlinear pulse evolution with reduced optical wave breaking in erbium-doped fiber amplifiers*, Optics Lett. **21**, 68 (1996).
- [Tau03] F. Tauser, A. Leitenstorfer, and W. Zinth, *Amplified femtosecond pulses from an Er:fiber system: Nonlinear pulse shortening and selfreferencing detection of the carrier-envelope phase evolution*, Opt. Express **11**, 594 (2003).
- [Tau04a] F. Tauser, *Frequenzkämme und weit abstimmbare Femtosekunden-Lichtimpulse im Nahen Infrarot aus einem kompakten Erbium-Faserlaser*, Ph.D. thesis, TU München (2004).
- [Tau04b] F. Tauser, F. Adler, and A. Leitenstorfer, *Widely tunable sub-30-fs pulses from a compact erbium-doped fiber source*, Opt. Lett. **29**, 516 (2004).
- [Tre02] R. Trebino, *Frequency-Resolved Optical Gating: The Measurement of Ultrashort Laser Pulses*, Kluwer Academic Publishers, 2002.
- [Ude99] T. Udem, J. Reichert, R. Holzwarth, and T. W. Hänsch, *Accurate measurement of large optical frequency differences with a mode-locked laser*, Opt. Lett. **24**, 881 (1999).
- [Ude02] T. Udem, R. Holzwarth, and T. W. Hänsch, *Optical frequency metrology*, Nature **416**, 233 (2002).
- [Wan09] B. Wang and E. Mies, *Review of Fabrication Techniques for Fused Fiber Components for Fiber Lasers*, SPIE Photonic West (2009).
- [Wid99] B. Widiyatmoko, K. Imai, M. Kourogi, and M. Ohtsu, *Second-harmonic generation of an optical frequency comb at 1.55  $\mu\text{m}$  with periodically poled lithium niobate*, Opt. Lett. **24**, 315 (1999).
- [Zha99] R. Zhang, D. Pang, J. Sun, Q. Wang, S. Zhang, and G. Wen, *Analytical expressions of group-delay dispersion and cubic phase for four-prism sequence used at other than Brewster's angle*, Optics & Laser Technology **31**, 373 (1999).



## Acknowledgments

First, I would like to thank my supervisor Hanns-Christoph Nägerl. On the one hand, for providing me with the opportunity to work in his group, on the other hand for giving me the possibility to go to Chicago for one year. Also, I would like to thank Rudolf Grimm, the head of our group.

I also have to thank Cheng Chin and his group at the University of Chicago. I had a great time and learned a lot. Especially, I want to thank Kathy-Anne Soderberg, Chen-Lung Hung, Xibo Zhang and last but not least Nathan Gemelke, who taught me a lot about physics and what the difference between hunting a tiger and clubbing a seal is.

I am very grateful for all the help I received from the CsIII-team. I would like to thank Hans Danzl for all the discussions about physics and recipes. Manfred Mark, who has been always willing to help me with non-working electronics and Elmar Haller, who basically knows everything about Matlab. I also want to thank my fellow diploma students, Lukas Reichsöllner, Oliver Krieglsteiner and Mohamed Rabie.

Before I started to built the laser, I had to learn how to splice fibers. Birgit Brandstätter taught me how to use the fusion fiber splicer and took care of the machine if something broke. Thank you.

I would also like to express my gratitude to the mechanical and the electronic workshop for all the machined parts and the electronic support. For the processing of all the orders, I really want to thank Sabine Hofer Brigo.

From the first semester on Adam Pauli and Johannes Schindler have been a great company and great friends. No matter what, skiing, biking, climbing, studying for exams, grinding coffee, making coffee, drinking coffee\*, it has always been a lot of fun.

And of course I would like to say a big thank you to my parents Josef and Margarete and my great girlfriend Myriam, who have always supported me in every possible way.

---

\*probably the best coffee in Innsbruck